Chapter II.3

Normal conducting magnets

Thomas Zickler
CERN, Geneva, Switzerland

This chapter aims to provide the guidance and tools necessary to carry out the analytical design of a simple accelerator magnet. As the chapter unfolds, we will explain some basic concepts, magnet types, and important aspects to consider before moving on to the actual design phase. The central part of this chapter is dedicated to a step-by-step explanation of how to develop a basic magnet design. We will cover a range of subjects like the layout of the magnetic circuit, excitation coils and cooling circuits, along with a short introduction to materials for the yoke and coil construction to complement this topic. The chapter also includes a practical part with problems and a case study for the reader to solve independently. Having worked through this chapter, the reader should be able to design an elementary magnet according to their needs.

II.3.1 Introduction

The goal of the JUAS lecture series *"Analytical and numerical design of normal-conducting accelerator magnets"* is to give an overview of the electromagnetic technology as used in and around particle accelerators and limited to normal-conducting iron-dominated electromagnets. In these lectures, we restrict our discussions to static current situations where we can assume that voltages generated by the change of flux and resulting eddy currents are negligible. Permanent and super-conducting magnet technologies are not covered there.

While the lectures deal with many more subjects like Maxwell's equations, numerical design, magnet manufacturing techniques, cost estimates, and quality assurance, this chapter concentrates only on the analytical design process. This restriction became necessary to ensure that this important subject is discussed with the required diligence without going beyond the scope of these proceedings. We consciously focus on applied and practical design aspects with the primary goal in mind to provide clear, workable instructions on how to approach the task of designing a standard accelerator magnet. These guidelines should also help to draft a list of critical parameters—with paper and pencil—without resorting to any complex computer programs.

Mathematics is reduced to a necessary minimum to keep it concise: The derivation of equations in this text might sometimes appear condensed. Should the reader need a more detailed and solid mathematical background, the references cited at the end of this chapter might help. We will systematically use SI units (MKSA) to guarantee consistency throughout the text, except when stated otherwise.

This chapter should be cited as: Normal conducting magnets, T. Zickler, DOI: 10.23730/CYRSP-2024-003.1001, in: Proceedings of the Joint Universities Accelerator School (JUAS): Courses and exercises, E. Métral (ed.),
CERN Yellow Reports: School Proceedings, CERN-2024-003, DOI: 10.23730/CYRSP-2024-003, p. 1001.

The chapter starts with a short overview of the most common magnet types and materials for magnet construction, followed by a section on design requirements and constraints. The central part introduces basic analytical magnet design, covering topics such as yoke design, coil dimensioning, and cooling layout.

A *case study* in the second part highlights this chapter's practical focus, allowing the readers to design a magnet on their own. For those willing to go deeper into the subject, the bibliography recommends scientific literature for further exploration.

II.3.2 Terms, definitions and conventions

For the sake of clarity, we will give definitions for the following terms and conventions.

II.3.2.1 Magnetic field

The *magnetic field* is a vector field that surrounds magnetised materials, electrical currents, and electrical fields varying in time and describes the magnetic influence on moving electrical charges and magnetic materials.

In the domain of electromagnetism, the term *magnetic field* is regularly used for two distinct but closely related vector fields, namely the *magnetic field strength* $\mathbf{H}$ and the *magnetic flux density* $\mathbf{B}$. While the definition of magnetic field is unambiguously defined and widely accepted, there is a certain confusion in the literature about the terms and definitions of magnetic field strength and magnetic flux density. Not claiming any universal validity, we define these terms within this chapter as follows:

The *magnetic field strength* $\mathbf{H}$ $[H] = 1\,\mathrm{A\,s^{-1}}$ is a physical quantity used to measure the intensity of a magnetic field and can be seen as the part of the magnetic field in a material that arises from an external current; its magnitude is independent of the type of the surrounding medium (not intrinsic to the material itself) [1].

The *magnetic flux density* $\mathbf{B}$ $[B] = 1\,\mathrm{T} = 1\,\mathrm{V\,s\,m^{-2}}$ is a separate physical quantity used to measure the intensity of a magnetic field and can be thought of as the response of a medium to the magnetic field strength $\mathbf{H}$. Magnetic flux density should not be confused with magnetic flux: The *magnetic flux* $\mathbf{\Phi}$ $[\Phi] = 1\,\mathrm{wb} = 1\,\mathrm{kg\,m^2\,A^{-1}\,s^{-2}}$ is defined as the surface integral of the flux density component perpendicular to this surface.

The total quantification of a magnetic field requires knowledge of the vector fields of both the magnetic field strength $\mathbf{H}$ and magnetic flux density $\mathbf{B}$. In vacuum, the vectors $\mathbf{H}$ and $\mathbf{B}$ at each point are oriented in the same direction and are directly proportional through

$$\mathbf{B} = \mu_0\,\mathbf{H}\,, \tag{II.3.1}$$

where μ_0 is the magnetic permeability of free space $\mu_0 = 4\pi \times 10^{-7}\,\mathrm{V\,s\,A^{-1}\,m^{-1}}$. In other media than free space, the vectors of the magnetic field strength $\mathbf{H}$ and magnetic flux density $\mathbf{B}$ can point in different directions yet follow the relation

$$\mathbf{B} = \mathbf{P_m} + \mu_0\,\mathbf{H} = \mu_0\left(\mathbf{H} + \mathbf{M}\right)\,, \tag{II.3.2}$$

where $\mathbf{P_m}$ is the magnetic polarization $[P_m] = 1\,\mathrm{T}$, and $\mathbf{M}$ is the magnetization $[M] = 1\,\mathrm{A\,m^{-1}}$.

The magnetization $\mathbf{M}$ is the vector field that expresses the density of permanent or induced magnetic dipole moments in magnetic material and is defined as the quantity of magnetic moment per unit volume. The magnetic polarization $\mathbf{P_m}$ is the magnetization $\mathbf{M}$ scaled by the magnetic permeability of free space μ_0.

In anisotropic materials, the three vectors $\mathbf{B}$, $\mathbf{H}$ and $\mathbf{P_m}$ can point in different directions, but always in such a way that the vector sum in Eq. (II.3.2) is fulfilled. For uniaxial magnetization, Eq. (II.3.2) can be simplified to a scalar form, which is widely used in engineering applications [2]:

$$B = \mu\, H\,. \tag{II.3.3}$$

The magnetic permeability μ in materials has always two components

$$\mu = \mu_0\, \mu_r\,, \tag{II.3.4}$$

where μ_r is the relative permeability, a dimensionless quantity representing the permeability of a specific medium. In vacuum, $\mu_r = 1$, so that H and B are strictly proportional. If μ_r is much larger than 1, we speak about ferromagnetic materials ($\mu_{\mathrm{iron}} > 1000$).

We can think about the magnetic field strength $\mathbf{H}$ as the part of the magnetic field produced only by electrical currents and the magnetic flux density $\mathbf{B}$ as the total magnetic field that also includes the contribution from the magnetic properties of the materials in the field. Although we define them differently, the term *magnetic field* will interchangeably be applied for both the magnetic field strength and magnetic flux density.

II.3.2.2 Polarity conventions

A positive current flows from the positive terminal of a power supply to the negative terminal. In this chapter, we will use the following colour convention: red for the electrical current entering the plane and blue for the current pointing out of the plane. The same convention is valid for the direction of charged particles.

The magnetic flux flows from the positive (North) pole to a magnet's negative (South) pole. The direction of the magnetic flux as a result of a positive electrical current in a coil is determined by the *right-hand rule*: When wrapping the right hand around the coil with the fingers in the direction of the electrical current, the thumb points in the direction of the magnetic south pole.

A similar rule exists to describe the effect of the Lorentz force

$$\mathbf{F} = q\,(\mathbf{E} + \mathbf{v} \times \mathbf{B})\,, \tag{II.3.5}$$

where q is the particle charge $[q] = 1\,\mathrm{C} = 1\,\mathrm{A\,s}$, $\mathbf{E}$ is the electric field vector $[E] = 1\,\mathrm{A\,m^{-1}}$, and $\mathbf{v}$ is the velocity vector $[v] = 1\,\mathrm{m\,s^{-1}}$ of the charged particle. We should remember that the direction of the particle motion has to be perpendicular to the magnetic field to see the Lorentz force. In other words, $\mathbf{v}$ and $\mathbf{B}$ create a plane, and $\mathbf{F}$ is perpendicular to this plane. When using the right-hand rule, this means that the index finger represents $\mathbf{v}$, the middle finger indicates the direction of $\mathbf{B}$, and the thumb points in the direction of the resulting force $\mathbf{F}$.

II.3.2.3 Coordinate system

To express the vector components of a magnetic field, we will use a right-handed, orthogonal coordinate system (x, y, z). The z-axis goes through the centre of the magnet aperture and is parallel to the trajectory of the particle beam. The positive z-axis points out of the plane. There is no universal definition of where $z = 0$ is located, but in practice, we will set it in the longitudinal centre of the magnet.

The x-axis and y-axis are the horizontal and vertical axes, respectively. Using a right-handed coordinate system, the positive curling motion of the x-axis towards the y-axis counterclockwise around the z-axis defines the positive directions of the x- and y-axis.

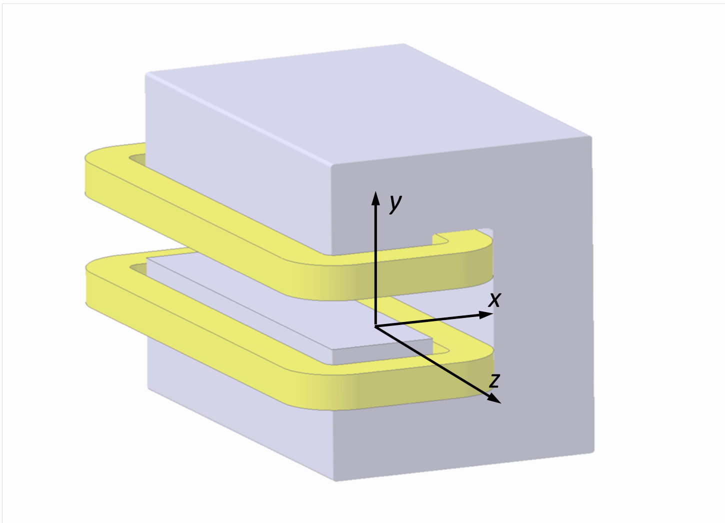

Fig. II.3.1: Right-handed, orthogonal magnet coordinate system (x, y, z) with the z-axis pointing in the direction of the particle trajectory.

II.3.2.4 Field description by multipoles

An arbitrary field vector $\mathbf{B}$ in a 2D-plane at a point defined by the complex coordinate $z = x + \mathrm{i}y$ can be represented by its vector components B_x and B_y with

$$\mathbf{B} = B_y + \mathrm{i}B_x \, .$$

Instead of describing the entire field in the aperture of a magnet by establishing a field map where we assign the vector components B_x and B_y to every single point in the plane, we can use a more elegant approach. Without providing a proof here in this chapter, the equation

$$\mathbf{B} = B_y + \mathrm{i}B_x = C_n \, z^{n-1} \tag{II.3.6}$$

with the complex coefficient

$$C_n = B_n + \mathrm{i}A_n$$

is a possible solution to Maxwell's equations for a magnetostatic situation in free space. In other words, we can describe a *complex field vector* by a *complex scalar coefficient* and the *complex position vector*. Magnetic fields that conform to this description are called *multipole fields*.

The complex number C_n has a real part B_n and an imaginary part A_n. If we consider only the real part B_n and neglect the imaginary part A_n, we speak about *normal* multipole fields (see Fig. II.3.2).

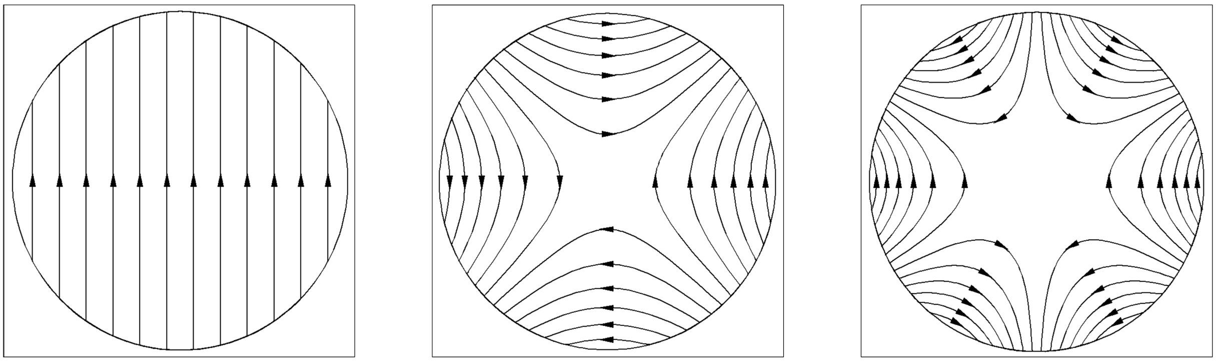

Fig. II.3.2: Normal multipole fields. Left: normal dipole with $B_1 = \mathrm{Re}\{C_1\}$. Middle: normal quadrupole with $B_2 = \mathrm{Re}\{C_2\}$. Right: normal sextupole with $B_3 = \mathrm{Re}\{C_3\}$.

The index n indicates the order of the multipole field: For example, if C_n is real and $n = 1$, we get a normal dipole field; for $n = 2$, we get a normal quadrupole field, and so on. On the x-axis, normal multipole fields involve only field components *perpendicular* to the x-axis, which suggests that the field is vertical in the horizontal plane.

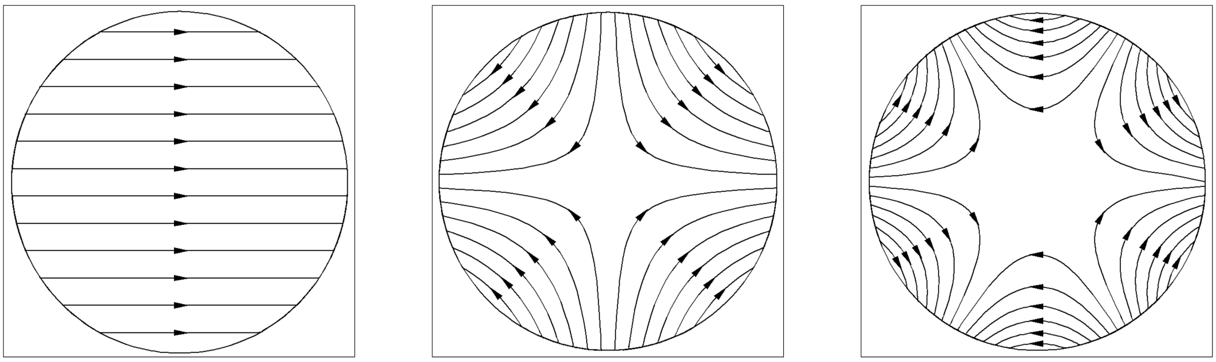

Fig. II.3.3: Skew multipole fields. Left: skew dipole with $A_1 = \mathrm{Im}\{C_1\}$. Middle: skew quadrupole with $A_2 = \mathrm{Im}\{C_2\}$. Right: skew sextupole with $A_3 = \mathrm{Im}\{C_3\}$.

On the other hand, if we consider only the imaginary part A_n we talk about *skew* fields. In the skew family, the field on the x-axis is always tangential to the x-axis, which means we have a horizontal field in the horizontal plane, as shown in Fig. II.3.3. The skew fields can be obtained from the normal ones with a rotation by $\pi/2n$; this means a rotation of 90° for a dipole and 45° for a quadrupole, and so on.

The *flux lines* of the magnetic field shown in Figs. II.3.2 and II.3.3 are also known as *vector equipotential lines* with the field vector always tangential to these flux lines. *Scalar equipotential lines* are orthogonal to the vector equipotential line. They define the boundary conditions for shaping the field (not shown here in these figures).

Since Maxwell's equations are linear, we can superpose any number of multipole fields and always obtain a valid solution to this equation. Hence, we can describe an arbitrary 2D vector field within a circle of validity $r_{\max}$ by a series of scalar coefficients

$$B_y + \mathrm{i}B_x = \sum_{n=1}^{\infty} (B_n + \mathrm{i}A_n) \left(\frac{x + \mathrm{i}y}{r_{\mathrm{ref}}}\right)^{n-1} . \tag{II.3.7}$$

These coefficients, B_n and A_n, are commonly named *multipole coefficients* and have units of tesla. The B_n-terms are the normal terms, whereas A_n-terms are called skew terms. The reference radius r_{ref} is used for normalisation, and when assigning a value to it, we choose one that defines the good-field region needed for the beam. A typical value is $2/3$ of the physical aperture. Since the value of B_n and A_n depend on r_{ref}, it is always necessary to attribute the value for r_{ref} together with the multipole coefficients.

It is important to highlight that this 2D multipole decomposition holds only within a region:

– without magnetic materials: in practice, this means in air or vacuum;
– without currents;
– when B_z is constant or zero.

We would theoretically need an infinite number of these coefficients for an accurate field reconstruction. Yet, in practice, we don't need all terms: A few coefficients in this convergent Fourier series are generally more than enough. We never practically go beyond $n = 20$, and in most cases, we terminate the series already at $n = 14$.

We should remember the following difference when defining the index n: In Europe, we go from 1 to ∞, but in the United States, the indexing starts from 0. This inconsistency could sometimes lead to confusion if you read papers written by colleagues from the United States.

II.3.3 Magnet types

This section gives an overview of the classical normal-conducting magnet types, highlights their main characteristics, and briefly explains their function and purpose in particle accelerators. In addition, we will show the most typical representatives of each type and explain their advantages and drawbacks. But before we do so, we will discuss the difference between coil-dominated superconducting magnets and iron-dominated normal-conducting magnets.

II.3.3.1 Magnet technologies

Accelerator magnets can fall into different categories and subcategories depending on the criteria applied. One of the criteria is the technology used to produce the magnetic field: We differentiate between electromagnets and permanent magnets. In electromagnets, the field is produced by electrical currents in the coil windings; in permanent magnets, the field is produced by hard magnetic materials. Permanent magnets are rarely used in particle accelerators mainly because they can only provide a constant field, in general. We can further distinguish electromagnets by the conductor technology applied: *superconducting* or *normal-conducting*.

Superconducting technology relies on superconducting materials as a conductor for the excitation current. These materials have zero electrical resistance at cryogenic temperatures and, therefore, no ohmic losses. Very high current densities can be achieved in the coils, but only with the help of cryogenic cooling.

For the construction of *normal-conducting* coils, resistive conductor materials like copper or aluminium are used, which sets a natural limit for the usable current densities due to ohmic losses and power dissipation in the coils—hence, only moderate current densities are possible.

Magnets can also be categorised based on how the magnetic field in the aperture is shaped. Simply speaking, we have two different ways to create a specific field distribution in the aperture of a magnet:

In *coil-dominated* magnets, the magnetic field in the aperture is shaped by the position of the conductors or, rather, the current distribution around the aperture. In coil-dominated magnets that need to generate magnetic fields of strength necessary for particle accelerators like the LHC, the current in the coils needs to be significant. These elevated currents are the reason why these magnets are often built from superconducting materials.

In contrast to coil-dominated magnets, the field distribution in the aperture of *iron-dominated* magnets is determined by the geometry of the iron poles, with the position of the coils being of minor importance for the strength and homogeneity of the field. The ideal pole profiles are curves of constant scalar potential with the flux lines perfectly perpendicular to these ideal iron poles. The field in iron-dominated magnets is limited to moderate field strength by saturation effects. So, resistive conductor materials are adequate to drive the magnetic flux in a magnetic circuit.

The two most widespread types are coil-dominated, superconducting magnets and iron-dominated, normal-conducting magnets. None of these technologies is superior to the other: Both types successfully co-exist because they are complementary in covering a more expansive field range.

II.3.3.2 Dipole magnets

In a circular particle accelerator or a curved beam transfer line, dipole magnets are the most commonly used elements. A dipole provides a uniform field between its two poles (North and South) excited by a current circulating in the coils. The system respects the right-hand convention—this means a current circulating counterclockwise around the poles produces a magnetic field that points upwards as indicated in Fig. II.3.4 (middle).

The purpose of dipole magnets is to bend or steer a charged particle beam. Following the right-hand rule, a beam of positively charged particles directed into the plane is deflected to the right when the magnetic field points upwards. This scheme is demonstrated in Fig. II.3.4 (right). The equation describing the ideal (infinite) pole profile for a normal (non-skew) dipole is

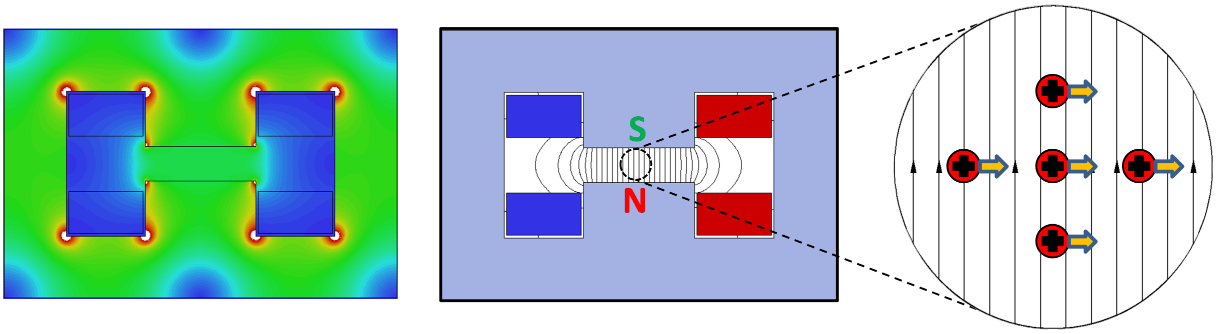

Fig. II.3.4: Normal dipole. Left: 2D field distribution of $|B|$. Middle: cross section, magnet polarity and corresponding flux lines in the aperture. Right: interaction with positively charged particles moving into the plane.

$$y = \pm r\,,$$

where r is the half-aperture height. The magnetic flux density between these two poles is ideally constant, as in Fig. II.3.4 (left), and has only a field component in y-direction:

$$B_x = 0 \quad \text{and} \quad B_y = B_1 = \text{constant}\,.$$

Although the design and layout of a dipole magnet can differ from case to case, depending on the application, we can identify three standard families, each with its advantages and drawbacks.

The *H-type magnet*, as shown in Fig. II.3.5, is fully symmetric, with a closed iron circuit and coils around the poles. Sharing the same field characteristics with the C-type magnet, this design is more compact and mechanically more stable—although at the cost of some access problems to the aperture, making the installation of coils and vacuum chamber more complicated. The coils can either sit in their coil window or extend to the mid-plane. In the latter case of the so-called bedstead coils, the coil heads must be bent upwards to clear the aperture region. In the specific case when the coils get close to the aperture, their position can negatively impact the field quality, especially at higher fields.

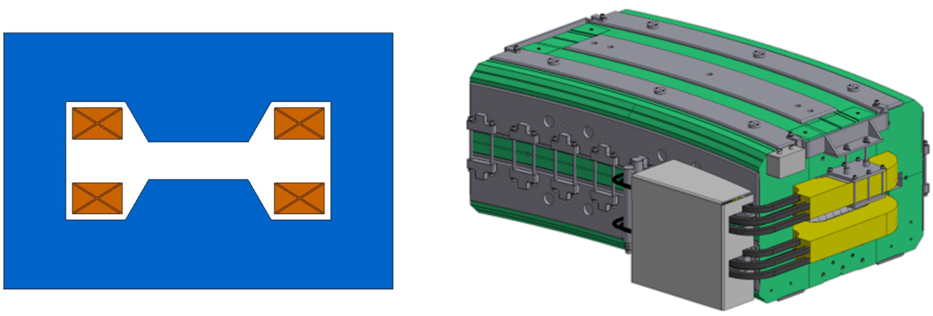

Fig. II.3.5: H-type dipole magnet: Due to its two-fold symmetry, this type provides a good magnetic field homogeneity.

Reducing the pole height to zero results in the *O-type* or *window-frame* magnet (see Fig. II.3.6) that is known for providing the best field quality due to the extra wide poles. Yet the particular design of the coils intrinsic to this magnet type makes the field quality sensitive to the correct positioning of the windings. The window-frame magnet has the same access problems as the H-type magnet.

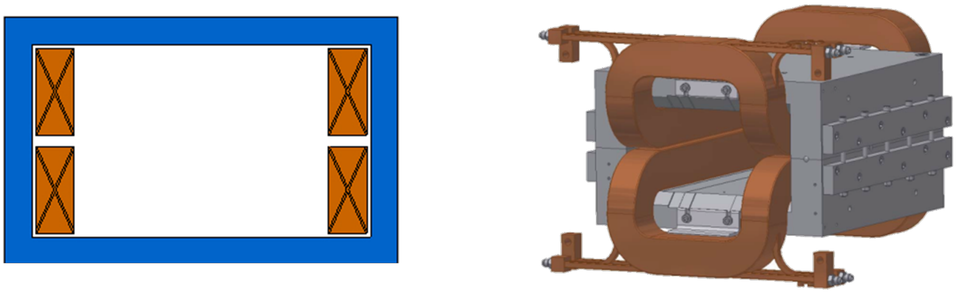

Fig. II.3.6: O-type or window-frame dipole magnet (type 1): Although providing an excellent magnetic field quality, the field quality is sensitive to the correct positioning of the coil windings.

Another variant of the window-frame magnet, shown in Fig. II.3.7, is often used as a layout for short magnets, like corrector or steering magnets, that can only produce a magnetic field of moderate strength. For the same flux density in the aperture, this type needs twice as many ampere-turns compared to type 1. This is a consequence of the fact that the coils are twined around the return legs, and the parts of the coils outside the yoke do not contribute to the magnetic field in the aperture—they just serve as a return path for the current.

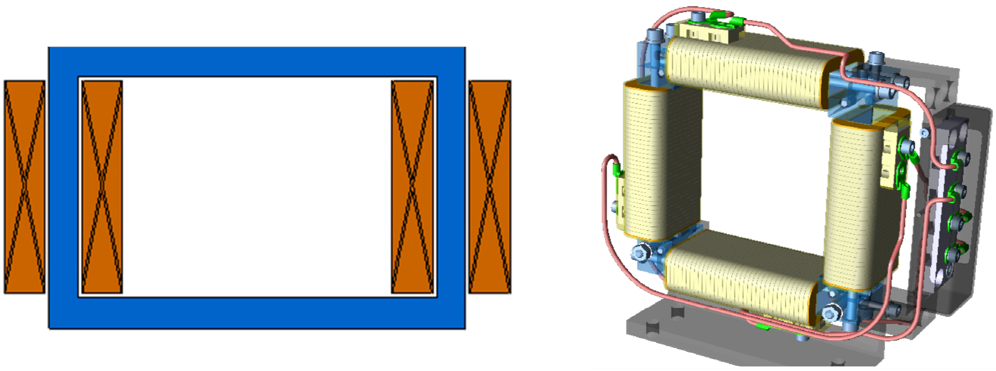

Fig. II.3.7: O-type or window-frame dipole magnet (type 2): This type is frequently used as a corrector or steering magnet.

As shown in Fig. II.3.8, the magnetic circuit of the *C-type* dipole is open on one side. This design offers excellent transversal accessibility to the magnet aperture and the beam pipe, thus making it a perfect candidate for light sources where the synchrotron light has to be extracted all along the circumference of the synchrotron. Due to its asymmetric layout, this magnet type is also suitable for injection and extraction regions or zones with adjacent beams very close to each other, such as the transfer lines of experimental areas.

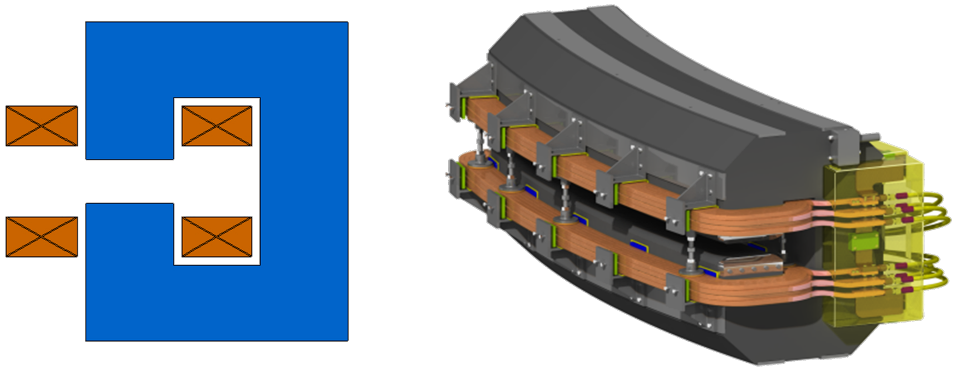

Fig. II.3.8: C-type dipole magnet: The particular design of this type makes it a perfect candidate for light sources where the synchrotron light has to be extracted all along the circumference of the synchrotron.

The yoke volume, and hence the weight of the C-type magnet, is considerably higher than that of the H-type magnet with a similar performance. Compared to the H-type or O-type magnet, the mechanical stability of the C-type is less good. When the magnet is pulsed, the attracting magnetic forces on the poles and its only one return leg may lead to a movement of the poles.

II.3.3.3 Quadrupole magnets

The second most commonly used magnetic element is the quadrupole magnet. Its purpose is to focus the beam. We should note that a horizontally focused beam is vertically defocused at the same time. The quadrupole magnet has four poles with a hyperbolic contour that can be described for a normal (non-skew) quadrupole by

$$2xy = \pm r^2 \,,$$

where r is the aperture radius.

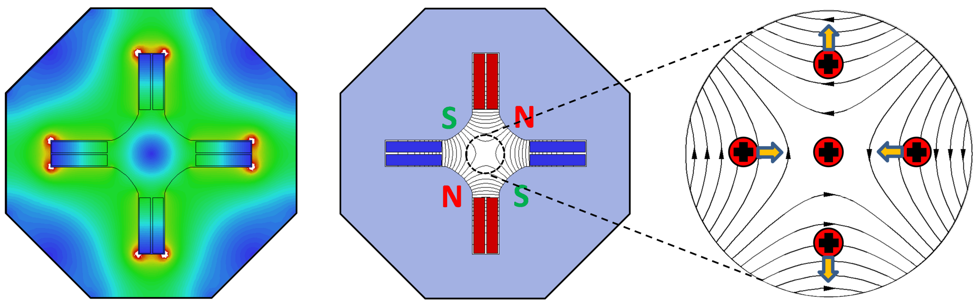

Fig. II.3.9: Normal quadrupole. Left: 2D field distribution of $|B|$. Middle: cross section, magnet polarity and corresponding flux lines in the aperture. Right: interaction with positively charged particles.

This type of magnet produces a zero magnetic field at the centre, and its intensity increases linearly with the radial distance. The equipotential lines are hyperbolas (xy = constant), and the field lines are perpendicular to them. The Cartesian components of the flux density in an ideal quadrupole are not coupled: The x-component of the flux density on a point in the aperture only depends on the y-coordinate, and the y-component only depends on the x-coordinate following the relation

$$B_x = \frac{B_2}{r_{\text{ref}}} y \quad \text{and} \quad B_y = \frac{B_2}{r_{\text{ref}}} x \,.$$

The characteristic parameter of the quadrupole is the field gradient G $[G] = 1\,\text{T}\,\text{m}^{-1}$, which is defined as

$$G = B' = \frac{B_2}{r_{\text{ref}}} = \frac{\mathrm{d}B}{\mathrm{d}r} \,.$$

With the polarity shown in Fig. II.3.9 (middle), the horizontal component of the Lorentz force on a positively charged particle moving into the plane is directed towards the axis; the vertical component is directed away from the axis. Figure II.3.9 (right) illustrates this horizontal focusing and vertical defocusing.

Like dipoles, quadrupoles come in different designs. The quadrupole in Fig. II.3.10 features four symmetric quadrants and 90° coils. Whereas the space for the coils is limited, the large poles ensure improved field quality.

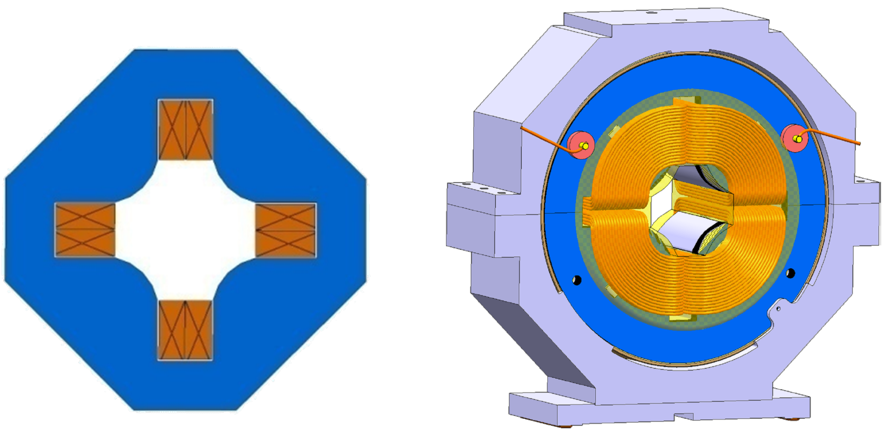

Fig. II.3.10: Quadrupole type 1 with 90° coils: The large poles ensure an improved field quality.

Figure II.3.11 shows a quadrupole with parallel poles and racetrack coils. The advantage of this design is a larger space for the coils. On the negative side, the smaller poles can lead to saturation on the pole roots, resulting in reduced field quality.

The third type (see Fig. II.3.12) is a so-called figure-of-eight or Collins quadrupole. It features a slim design and openings on the sides, allowing the radial extraction of beams or synchrotron light. As a result of the missing vertical back legs, this design is obviously mechanically less stable and more expensive to produce. Like the C-type dipole, the Collins quadrupole can often be found in light sources and beam transfer lines.


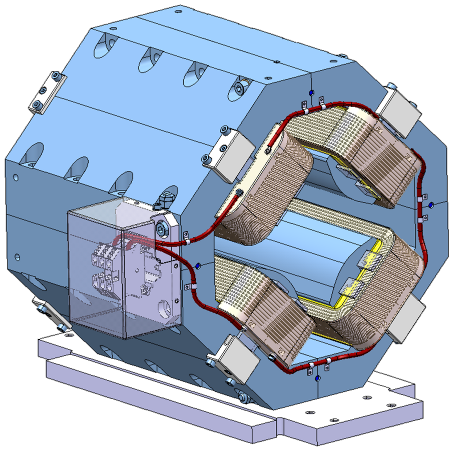

Fig. II.3.11: Quadrupole type 2 with parallel poles: The advantage of this design is the enlarged space for the coils.

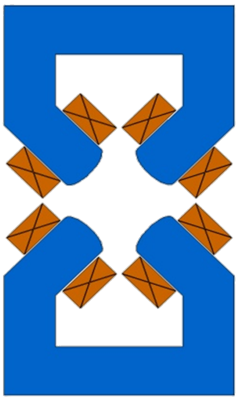
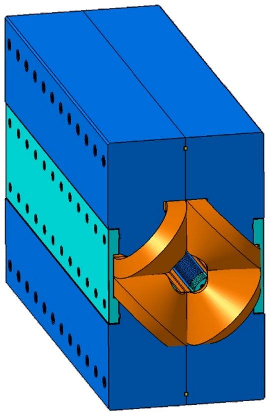

Fig. II.3.12: Figure-of-eight or Collins quadrupole: The slim design makes this type suitable for transfer lines with limited transversal space.

II.3.3.4 Sextupole magnets

Sextupole magnets, which have six poles of round or flat shape, are used in circular accelerators and less often in transfer lines. Their primary function is to correct chromatic aberrations in accelerators. Off-momentum particles are incorrectly focused in quadrupoles, which means that in the case of high-momentum particles with higher beam rigidity, the beam is underfocused, leading to the distortion of betatron oscillation frequencies.

A positive sextupole field can correct this effect: Off-momentum particles circulate with a radial displacement with respect to the central orbit and see, therefore, a correcting field in the sextupole as shown in Fig. II.3.13 (right) reducing the chromaticity to zero. An analogous principle applies to over-focused low-momentum particles. The equation for a normal (non-skew) sextupole with ideal poles is

$$3x^2y - y^3 = \pm r^3 ,$$

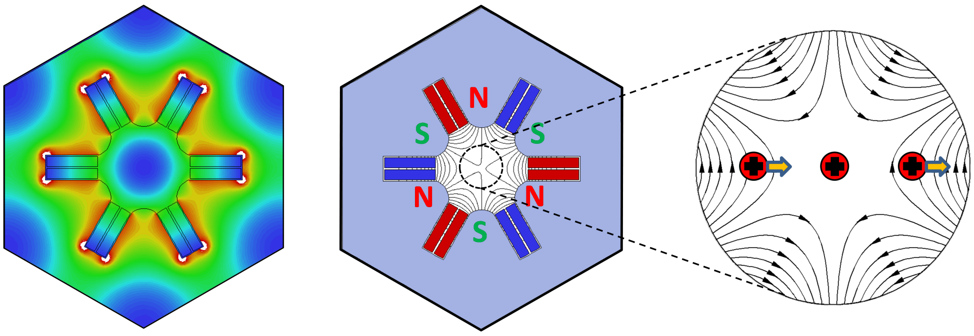

Fig. II.3.13: Normal sextupole. Left: 2D field distribution of $|B|$. Middle: cross section, magnet polarity and corresponding flux lines in the aperture. Right: interaction with positively charged particles.

where r is the aperture radius. However, a simple circular arc often approximates the pole profile of a sextupole.

The magnetic field varies quadratically with the radial distance from the magnet centre. Sextupoles are non-linear beam-optics elements, which means that the y-component of the flux density at a certain point in the aperture depends on both the x- and y-coordinate and is described by

$$B_x = \frac{B_3}{r_{\text{ref}}^2} xy \quad \text{and} \quad B_y = \frac{B_3}{r_{\text{ref}}^2} \left(x^2 - y^2\right) .$$

The characterising parameter of the sextupole is the second derivative of the field:

$$B'' = \frac{2\,B_3}{r_{\text{ref}}^2} = \frac{\mathrm{d}^2 B}{\mathrm{d}r^2} .$$

II.3.3.5 Skew magnets

In the previous section, we have dealt with magnets capable of producing either a normal or a skew field—an intrinsic quality irrespective of their multipole order. A skew field is a result of rotating a normal field along the longitudinal axis by $\pi/2n$. A rotation of a quadrupole produces skew quadrupole components and, therefore, leads to some linear betatron coupling.

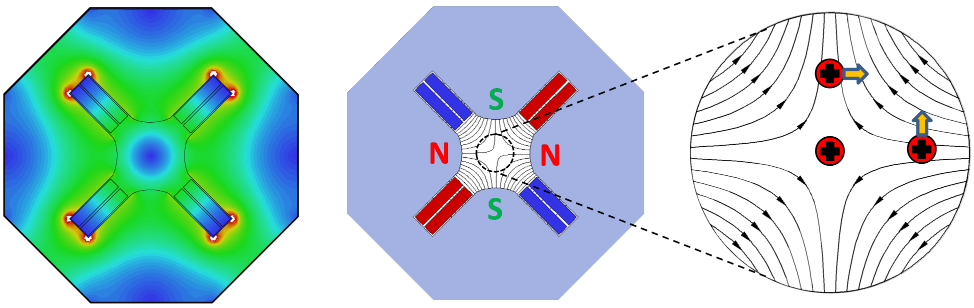

Fig. II.3.14: Skew quadrupole. Left: 2D field distribution of $|B|$. Middle: cross section, magnet polarity and corresponding flux lines in the aperture. Right: interaction with positively charged particles.

Figure II.3.14 demonstrates a skew quadrupole—its purpose is to control the coupling of horizontal and vertical betatron oscillations. In a skew quadrupole, a beam that is displaced in the horizontal plane is deflected vertically, and a beam that is displaced in the vertical plane is deflected horizontally.

II.3.4 Materials

This chapter will give an overview of the characteristics and properties of materials used for magnet manufacturing, such as ferromagnetic materials and electrical conductors. Although most readers will probably never build a magnet with their own hands, it is essential to have a basic knowledge of material characteristics as they directly impact the preceding design process.

II.3.4.1 Yoke materials

Magnetic circuits or magnet yokes are made from materials with a high relative permeability $\mu_r \gg 1$, called ferromagnetic materials. In particular, soft ferromagnetic materials are of interest—the metals that can be easily magnetised and demagnetised feature a high permeability, a narrow hysteresis loop, and a high magnetic saturation induction.

II.3.4.1.1 Solid vs. laminated yokes

Iron-dominated magnets can be built from massive iron blocks, which makes them sensitive to eddy currents. This undesired effect prevents them from being pulsed or cycled rapidly. To reduce or avoid eddy currents in pulsed operation, the yoke has to be laminated. In the past, the decisive factor in selecting the yoke material—laminated or solid steel—was the requirement for the magnet to be operated either in a cycled or static mode. Nowadays, most magnets are commonly manufactured from laminated steel.

Unlike laminated yokes, those machined from cast ingots require no specific tooling. A significant problem with massive yokes is the difficulty of building a series of magnets with similar magnetic performance.

Admittedly, yokes built from steel sheets are more labour-intensive and require expensive tooling for stamping, stacking and assembling. That said, there are a lot of manufacturing and operational advantages when opting for steel sheets over solid iron blocks: Steel sheets are less expensive than blocks; the magnetic and mechanical properties can be adjusted by final annealing; the steel quality is reproducible even in large series production; the magnetic properties (permeability, coercivity) remain within small tolerances. Last but not least, laminated magnets are less expensive for larger series because the tooling is part of the fixed costs: the more magnet units are produced, the smaller the contribution of the tooling to the total costs.

II.3.4.1.2 NGO electrosteel

One of the most common materials for laminated magnets is fully annealed, cold-rolled, non-grain oriented (NGO) electrosteel as defined in DIN EN10106 [3]. Table II.3.1 summarises typical material properties of cold-rolled NGO electrosteel. More detailed information on specific materials can be requested from steel producers.

Table II.3.1: Typical properties of cold-rolled NGO electrosteel.

Property	Typical value
Steel thickness	$0.3 \leq t \leq 1.5\,\mathrm{mm}$
Density	$7.60 \leq \delta \leq 7.85\,\mathrm{g\,cm^{-3}}$
Coercivity	$H_c < 65\,\mathrm{A\,m^{-1}}$
Coercivity spread	$\Delta H_c < \pm 10\,\mathrm{A\,m^{-1}}$
Electrical resistivity at 20°C	$0.16\,(\text{low Si}) \leq \rho \leq 0.61\,\mu\Omega\,\mathrm{m}\,(\text{high Si})$

II.3.4.1.3 Insulation coating

Like in solid yokes, eddy currents can also be present in laminated yokes if there is an electrical contact between the stacked laminations. The individual laminations should be coated on one or both sides with a micrometre-thin insulation layer to avoid this undesired effect.

Apart from the classical coating techniques, like blue steaming or phosphatization, steel suppliers nowadays offer a wide range of organic and inorganic coatings with different properties. Some epoxy-based coatings provide electrical insulation and act as a bonding agent to glue the individual laminations together at the same time. This distinguishing characteristic makes them particularly interesting for manufacturing laminated yokes because it offers an alternative assembly technique without welding involved.

II.3.4.1.4 Steel permeability and saturation

At the beginning of this chapter, we have discussed the relation between the magnetic field strength H and magnetic flux density B. This relation is called permeability μ and consists of two components: the permeability of free space μ_0 and the relative permeability μ_r. The latter, a dimensionless quantity describing the magnetic behaviour of materials, is large in ferromagnetic materials (sometimes as high as 10 000) but not constant—it changes as a function of the flux density. We can see this non-linearity in Fig. II.3.15 (left), where the magnetic induction B as a function of the magnetic field strength H is plotted for different ferromagnetic materials. This plot is called the $B(H)$ curve.

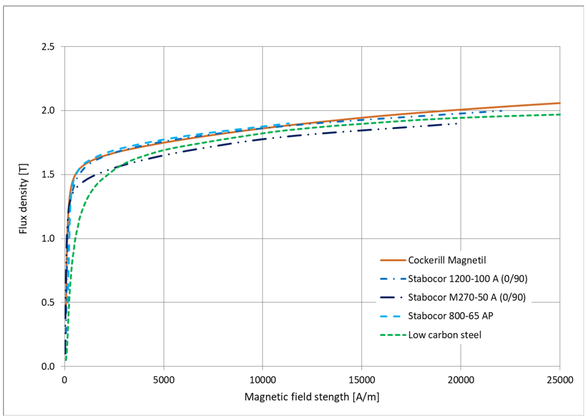

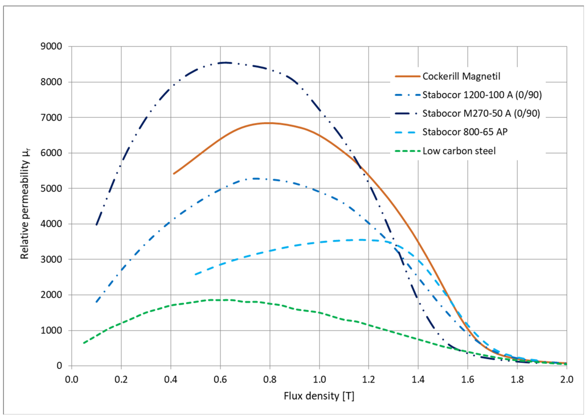

Fig. II.3.15: Non-linear permeability for different magnetic steel types. Left: Flux density B as a function of magnetic field strength H. Right: Relative permeability μ_r as function of flux density B.

The non-linearity appears even more apparent when we plot the permeability as a function of the magnetic flux density, as shown in Fig. II.3.15 (right). If we look at very high induction levels, the permeability is significantly reduced, an effect known as *saturation*. This reduction in permeability is also true for the low-induction region.

From these curves, we can conclude that increasing flux density B above $1.5 - 1.6\,\mathrm{T}$ in iron requires a non-proportional field strength H increase. We should remember that ignoring the above-mentioned relation may cause saturated areas in the iron yoke. Saturation means a local decrease in relative permeability (small μ_{iron}), which can lead to inefficiencies of the magnetic circuit.

By analogy with electrical circuits, we can define the resistance of a magnetic circuit called magnetic reluctance $R_m [R_m] = 1\,\mathrm{H}^{-1} = 1\,\mathrm{A}^2\,\mathrm{s}^2\,\mathrm{kg}^{-1}\,\mathrm{m}^{-2}$. The equivalent of Ohm's law for electrical circuits, Hopkinson's law describes the relation between the magnetomotive force NI and the resulting magnetic flux Φ:

$$R_m = \frac{NI}{\Phi} = \frac{\lambda_m}{a_m\,\mu_o\,\mu_r}\,, \tag{II.3.8}$$

with λ_m being the flux path length $[\lambda_m] = 1\,\mathrm{m}$ and a_m the iron cross section perpendicular to the flux $[a_m] = 1\,\mathrm{m}^2$.

II.3.4.1.5 Steel anisotropy

Ferromagnetic materials have another particularity related to the production process and its impact on the crystal structure. As a result of the cold rolling process, electrosteel sheets show an anisotropy in their material properties, especially in permeability. Parallel to the rolling direction, the permeability is higher than perpendicular to the rolling direction. Although this anisotropy can be reduced to a certain extent during the annealing process, the steel sheets will never become fully isotropic.

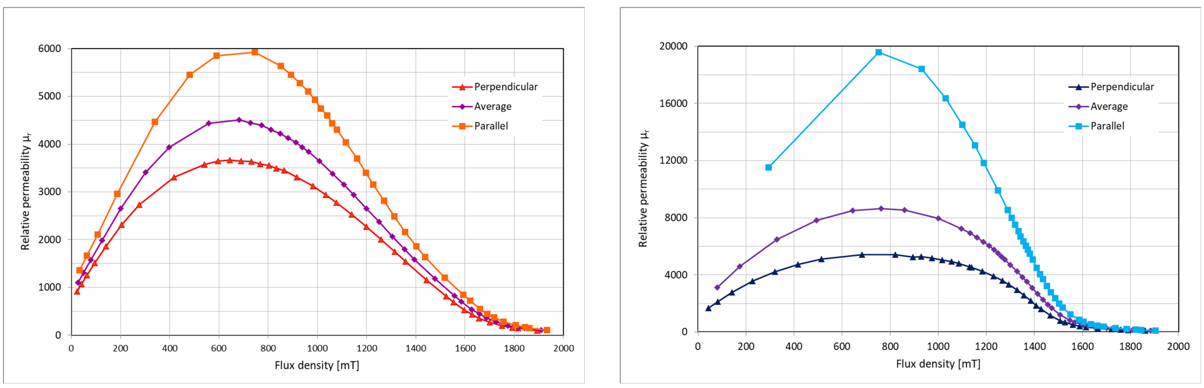

Fig. II.3.16: Anisotropy of standard cold-rolled NGO steel grades. The permeability depends on the orientation with respect to the rolling direction. Left: grade M1300-100A. Right: grade M250-35HP (high permeable material).

Figure II.3.16 (left) shows the anisotropic permeability of standard cold-rolled NGO steel of 1 mm thickness commonly used for yoke fabrication (grade M1300-100A). This steel grade has a low carbon as well as relatively low silicon contents. The permeability in the rolling direction is almost twice as high as that measured perpendicular to the rolling direction. This effect is even more pronounced in high permeable materials like M 250-35 HP as shown in Fig. II.3.16 (right). This 0.35 mm thick steel has a high silicon content that increases both the permeability and resistivity and decreases the coercivity at the same time. The permeability in the two directions differs by a factor of more than three. In grain-oriented (GO) materials, the anisotropy is even more pronounced.

This particularity of cold-rolled NGO steel impacts the manufacturing process. When stamping the laminations, their orientation with respect to the rolling direction is fundamental. Ignoring the anisotropy of the magnetic properties can lead to asymmetries in magnetic flux distribution thus violating the symmetry conditions in a magnet.

II.3.4.1.6 Hysteresis, remanence and coercivity

In ferromagnetic materials, we can observe that the flux density B as a function of the field strength H is different, depending on whether the excitation is increasing or decreasing (see Fig. II.3.17). This effect is called hysteresis and can be explained by the complex, intrinsic processes—movements and growth of magnetic domains—in ferromagnetic materials when subject to an external magnetic field.

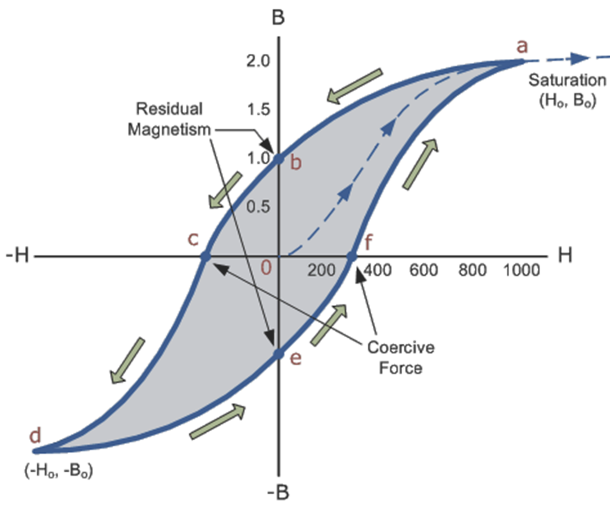

Fig. II.3.17: Hysteresis: the flux density B as a function of the field strength H is different, depending on whether the excitation is increasing or decreasing.

With the excitation current switched off and zero magnetic field strength H as a result, there is still some magnetic polarization remaining in the iron: This phenomenon is called *remanent magnetic flux density* or *magnetic remanence* B_{rem}. The width of the hysteresis curve is determined by the coercive force or coercivity H_c. The quantity H_c is defined as a value of the field strength that reduces the magnetic flux density in steel to zero. Materials having $H_c < 1000\,\mathrm{A\,m^{-1}}$ are known as soft magnetic, and materials with $H_c > 1000\,\mathrm{A\,m^{-1}}$ are called hard magnetic (see Fig. II.3.18). We are mostly interested in soft magnetic materials for the construction of magnetic circuits. Hard magnetic materials are used to produce permanent magnets.

II.3.4.2 Coil materials

Conductor materials that are commonly used for the construction of normal-conducting coils include aluminium and copper. Both materials are available in different grades and purities. The material prop-

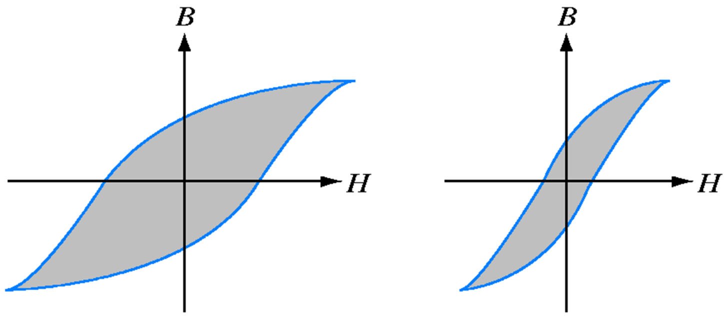

Fig. II.3.18: The coercive force determines the width of the hysteresis curve. Left: hard magnetic material with $H_c > 1000\,\mathrm{A\,m^{-1}}$. Right: soft magnetic material with $H_c < 1000\,\mathrm{A\,m^{-1}}$.

erties of two typical standard grades—pure aluminium and oxygen-free (OF) copper—are summarised in Table II.3.2. Magnet designers and engineers looking for more detailed information and other available grades should consult suppliers, material databases, or international standards.

While aluminium was a good alternative in the past thanks to its low price, copper coils are more state-of-the-art nowadays. Assuming the electrical resistance in coils is the same, the material costs of copper and aluminium coils are comparable today. However, the higher electrical conductivity of copper means more compact coil dimensions, leading to a smaller magnet overall.

Table II.3.2: Typical properties of standard conductor materials.

Property	Aluminium	Oxygen-free (OF) Copper
Purity	99.7%	99.95%
Density	$2.70\,\mathrm{g\,cm^{-3}}$	$8.94\,\mathrm{g\,cm^{-3}}$
Electrical resistivity at 20°C	$2.83\,\mu\Omega\,\mathrm{m}$	$1.72\,\mu\Omega\,\mathrm{m}$
Temperature coefficient of resistance	$0.004\,\mathrm{K^{-1}}$	$0.004\,\mathrm{K^{-1}}$
Thermal conductivity	$2.37\,\mathrm{W\,cm^{-1}\,K^{-1}}$	$3.91\,\mathrm{W\,cm^{-1}\,K^{-1}}$

When winding a coil—whether made of aluminium or copper—we have to avoid small bending radii. A tight bending increases the risk of insulation damage, decreases the cross section of the cooling duct and leads to a larger outer dimension of the conductor, known as *keystone effect*.

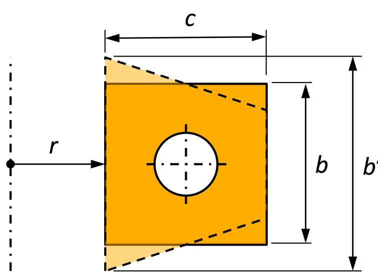

Fig. II.3.19: The keystone effect can lead to a significant deformation of the conductor when the bending radius becomes too small.

The keystone effect, as demonstrated in Fig. II.3.19, is a deformation of the conductor in the direction parallel to the bending axis. This results in a growth of the conductor dimension on the inner bending radius of the coil. For square conductor cross sections, this effect is empirically quantified as follows:

$$\text{if} \quad r = 3\,c \quad \Rightarrow \quad \frac{\Delta b}{b} = \frac{b' - b}{b} = 3.6\%\,.$$

For a bending radius of three times the conductor width c, we can expect a conductor growth of 3.6%, where c is the conductor dimension perpendicular to the bending axis. In the case of coils with many turns, the cumulative effect can lead to a significantly increased coil size in the bending regions and, consequently, to installation problems in the yoke. In principle, we can neglect the keystone effect by systematically choosing a bending radius three times larger than the conductor width c. This rule holds for all square or nearly square conductor cross sections; rectangular conductors bent around the shorter side show a more pronounced keystone effect.

II.3.5 Magnet design

Before discussing magnet design, we need to collect all the relevant information that will influence the design, construction, installation, and operation of the future magnet. This section explains what "relevant" means and is preceded by a brief discussion of goals in magnet design and magnet life cycles.

II.3.5.1 Design process

The flow diagram in Fig. II.3.20 shows the typical life cycle of a magnet: from the design and construction with its subsequent installation and operation to its final disposal or destruction. We will concentrate mainly on the part related to design and calculations. This phase can be split into different steps following a more or less sequential order with possible feedback loops at certain stages. At the beginning of each project, the requirements, constraints, and boundaries must be defined. This set of parameters serves as a starting point for the first analytical design to be followed by a basic numerical design. After each sequential step (electrical design, mechanical design, integration assessment, and cost estimation), one or more iterations of the analytical design might become necessary. Once these steps deliver satisfactory results, we can launch an advanced numerical design that includes field optimisation.

II.3.5.2 Input parameters

It is essential to realise that a magnet is not a stand-alone device. Along its life cycle, a magnet interacts with other devices and its environment. In close cooperation with corresponding work packages, the magnet designer must ensure that these interactions are fully considered in the early design phase. Ignoring any of the critical aspects may result in the avoidable necessity of implementing difficult modifications to the finished product.

The main work packages are summarised in Fig. II.3.21. Some of them, like beam optics, power converters, and cooling work packages, are obvious partners to be involved in magnet design from the very beginning. Others, such as vacuum, survey and integration teams, are often contacted at a later

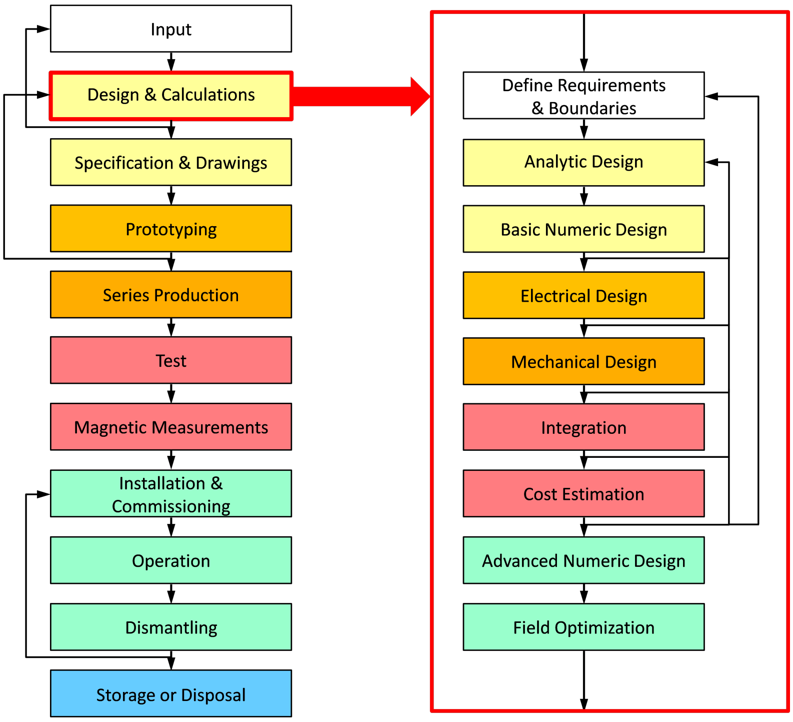

Fig. II.3.20: Left: Life cycle of a magnet. Right: Design phase with different steps.

stage of the project—sometimes too late and unnecessarily complicating the life of the concerned parties. Examples of work packages most likely to be forgotten are safety and transport. As a result, substantial and expensive engineering modifications might become necessary to install and operate a magnet safely.

It is good practice to contact the responsible partners, collect all necessary information, understand the requirements, constraints, and interfaces, and summarise them in a functional specification that each involved party should approve before starting the actual design work. Table II.3.3 lists the most relevant aspects that need to be considered by a magnet designer before starting the design work.

II.3.6 Analytical design

Before moving on to a detailed numerical magnetic field study calculating the field distribution and field quality of complex magnetic assemblies, we should focus on a basic analytical and conceptual design. Such an approach allows us to derive the most important characteristics and parameters of a future magnet with relatively good accuracy. The outcome of the analytical design process will serve as a solid foundation for the ultimate numerical design, thus reducing the number of design iterations.

A magnet is an assembly of different components. Figure II.3.22 shows two typical normal-conducting iron-dominated magnets—an air-cooled quadrupole (left) and a water-cooled quadrupole (right)—and their main components: the magnetic circuit, the excitation coils, the cooling circuit, the alignment targets, the interlock sensors, the electrical and hydraulic connections, and the magnet support.

In the following sections, we will explain how to design the magnetic circuit and coils and dimension the cooling circuits. The other components will not be discussed here since they have no direct influence on the magnet performance but are part of the mechanical design.

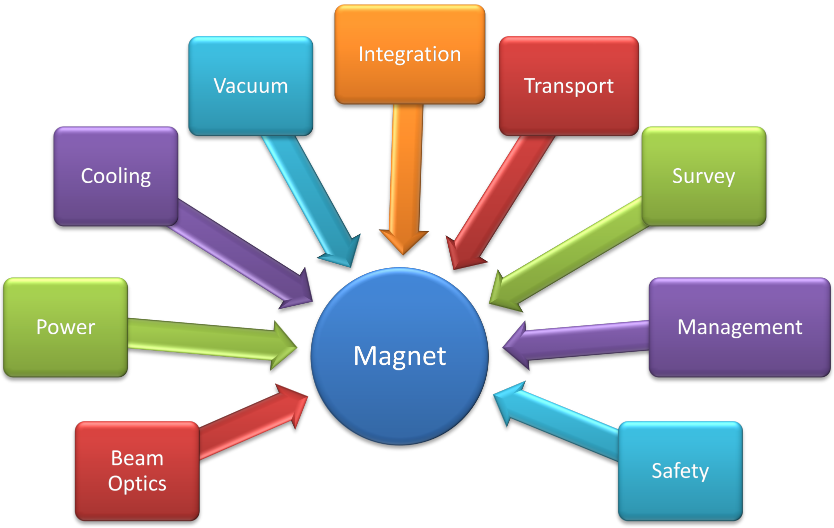

Fig. II.3.21: Magnet interaction partners.

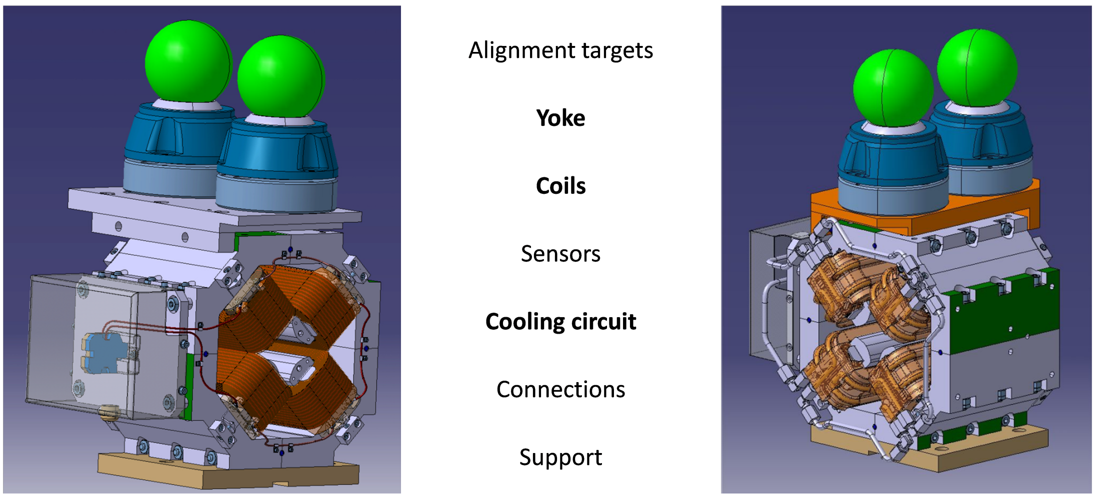

Fig. II.3.22: The main components of an accelerator magnet include the magnet yoke and coils, but also alignment equipment, interlock components, electrical and hydraulic connections, and adjustable supports. Left: air-cooled quadrupole. Right: water-cooled quadrupole.

II.3.6.1 Yoke design

The first step in the yoke design process is to derive the geometry of the magnetic circuit from beam-optic requirements. This means we have to define the yoke characteristics such as magnetic induction, aperture size, and magnet excitation (ampere-turns). Magnetic flux density is one of the most relevant parameters of a magnet. To determine the required flux density, we need to enter into the subject of beam optics, as explained in the section below.

Table II.3.3: Important aspects to be considered by the magnet designer.

General requirements	Magnet type and purpose Application Quantity & spare policy
Performance requirements	Beam parameters Requirements on field quality Magnet aperture and good-field region Operation mode
Physical requirements	Geometric boundaries Transport & handling Survey & alignment Accessibility
Interfaces	Power converter Cooling Vacuum Machine protection
Environmental aspects	Temperature Ionising radiation electromagnetic compatibility Safety

II.3.6.1.1 Beam rigidity

A good starting point to define the necessary magnetic induction is determining the beam rigidity as a function of the particle type and the envisaged beam energy [4]. The beam rigidity, which describes the stiffness of a beam, can be seen as the resistance of a particle beam against a change of direction when applying a bending force and is defined as

$$B_\rho = \frac{p}{q} = \frac{1}{q\,c}\sqrt{E_k^2 + 2\,E_k\,E_0}\,, \tag{II.3.9}$$

where B_ρ is the beam rigidity $[B_\rho] = 1\,\mathrm{T\,m}$, p is the particle momentum $[p] = 1\,\mathrm{kg\,m\,s^{-1}}$, q is the particle charge $[q] = 1\,\mathrm{C} = 1\,\mathrm{A\,s}$, c is the speed of light with $c = 299.792 \times 10^6\,\mathrm{m\,s^{-1}}$, E_k is the kinetic energy of the particle $[E_k] = 1\,\mathrm{J}$, and E_0 is the particle rest mass energy $[E_0] = 1\,\mathrm{J}$.

II.3.6.1.2 Flux density

From the beam rigidity and the magnet's bending radius, we can calculate the dipole magnet's flux density B.

$$B = \frac{B_\rho}{r_m}\,, \tag{II.3.10}$$

with r_m being the magnet bending radius $[r_m] = 1\,\mathrm{m}$. Analogous to the dipole, the required quadrupole field gradient G can be derived by using

$$G = B' = B_\rho \, k \, , \tag{II.3.11}$$

where k is the quadrupole strength $[k] = 1\,\mathrm{m}^{-2}$. Similarly, the differential field gradient B'' of a sextupole can be computed as follows:

$$B'' = B_\rho \, j \, , \tag{II.3.12}$$

with j being the sextupole strength $[j] = 1\,\mathrm{m}^{-3}$.

II.3.6.1.3 Aperture size

The aperture size of a magnet, as presented in Fig. II.3.23, is mainly determined by the central region around the theoretical beam trajectory. Referred to as good-field region (GFR), it specifies an area with a field quality within specific tolerances. The good-field region characterised by different shapes—circular, rectangular or elliptical—includes the maximum beam size as well as a certain margin for closed orbit distortions.

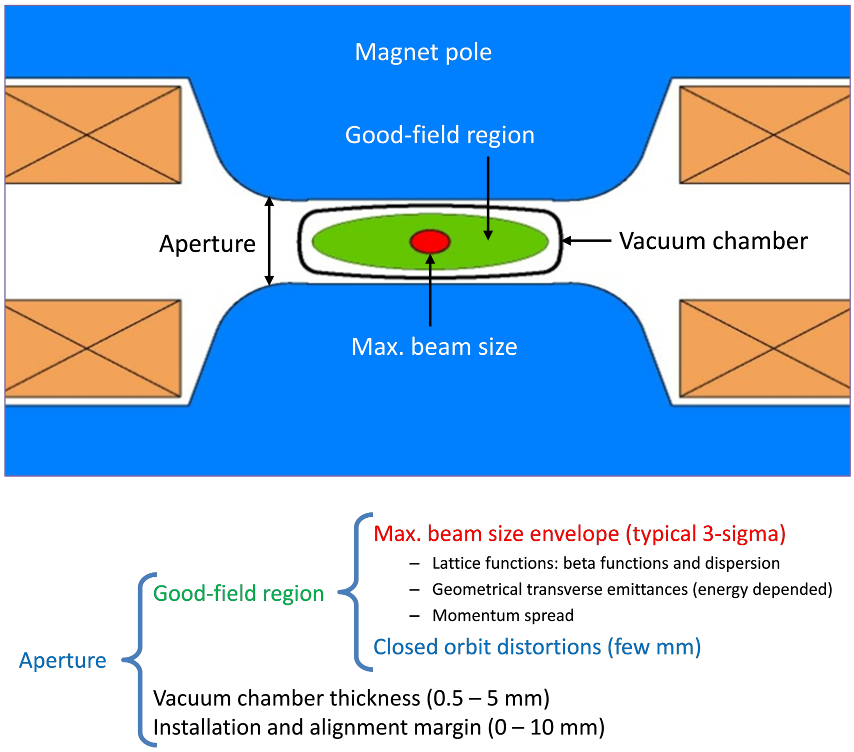

Fig. II.3.23: The physical (mechanical) magnet aperture includes the good-field region, the thickness of the vacuum chamber and some margin for installation and alignment.

The calculation of maximum beam size σ can be made with the help of Eq. (II.3.13) based on the lattice functions (beta functions β and dispersion D), energy dependent transverse emittance ε, and momentum spread $\Delta p/p$:

$$\sigma = \sqrt{\varepsilon\,\beta + \left(D\frac{\Delta p}{p}\right)^2}\,. \tag{II.3.13}$$

The largest beam size can be expected at injection energy, where the beam envelope typically measures a few σ. The total required aperture size is the sum of the good-field region, the vacuum chamber thickness (0.5–5.0 mm) and a margin for installation and alignment (0–10 mm). This is illustrated in Fig. II.3.23. We should remember that the numbers quoted here present typical values for synchrotrons indicating the order of magnitude. Depending on the individual case, actual values can significantly vary from the quoted numbers, particularly for the material thickness of vacuum chambers. For a straight, short vacuum chamber made of stainless steel with a circular cross section, a thickness of $1.0 - 2.0$ mm is sufficient, while a long aluminium chamber with a racetrack cross section requires a corrugated chamber wall, which can easily reach a thickness of $5 - 10$ mm.

II.3.6.1.4 Excitation current

Knowing a magnet's aperture, we can calculate the excitation current in coils required to produce the desired field strength.

Dipole magnets

For a dipole, we can work out the necessary ampere-turns by applying Ampere's law:

$$\oint \mathbf{H}\,\mathrm{d}\mathbf{s} = NI \tag{II.3.14}$$

and

$$\mathbf{B} = \mu\mathbf{H} \tag{II.3.15}$$

and

$$\mu = \mu_0\,\mu_r\,. \tag{II.3.16}$$

We can integrate B along a closed path as shown in Fig. II.3.24. Assuming that B remains constant all along this path, we can split the integration path into two parts: one in the magnet aperture $s_1 = h$, the other in the iron circuit s_2. Solving the integrals leads to

$$\begin{aligned} NI &= \oint \frac{\mathbf{B}}{\mu}\,\mathrm{d}\mathbf{s} \\ &= \int_{s_1} \frac{\mathbf{B}}{\mu_{\mathrm{air}}}\,\mathrm{d}\mathbf{s} + \int_{s_2} \frac{\mathbf{B}}{\mu_{\mathrm{iron}}}\,\mathrm{d}\mathbf{s} \\ &= \frac{B\,h}{\mu_{\mathrm{air}}} + \frac{B\,\lambda_{\mathrm{iron}}}{\mu_{\mathrm{iron}}}\,. \end{aligned} \tag{II.3.17}$$

In Eq. (II.3.17), the integration path in the aperture is expressed by h and the mean flux path in the iron circuit by λ_{iron}. As long as the iron is not saturated, we can further assume that

$$\frac{h}{\mu_{\text{air}}} \gg \frac{\lambda_{\text{iron}}}{\mu_{\text{iron}}} \tag{II.3.18}$$

such that Eq. (II.3.17) can be simplified to

$$NI \cong \frac{B\,h}{\mu_0}\,, \tag{II.3.19}$$

where h is the full aperture height $[h] = 1\,\text{m}$ and NI are the total ampere-turns $[NI] = 1\,\text{A}$. We should bear in mind that Eq. (II.3.19) only offers an approximate solution while neglecting fringe fields and iron saturation. In order to account for these effects, we should extend Eq. (II.3.19) with an efficiency factor η typically between 97% and 99%, depending on the design. This leads to the following equation, this time with the ampere-turns per coil:

$$NI_{(\text{per pole})} = \frac{B\,h}{2\,\eta\,\mu_0}\,. \tag{II.3.20}$$

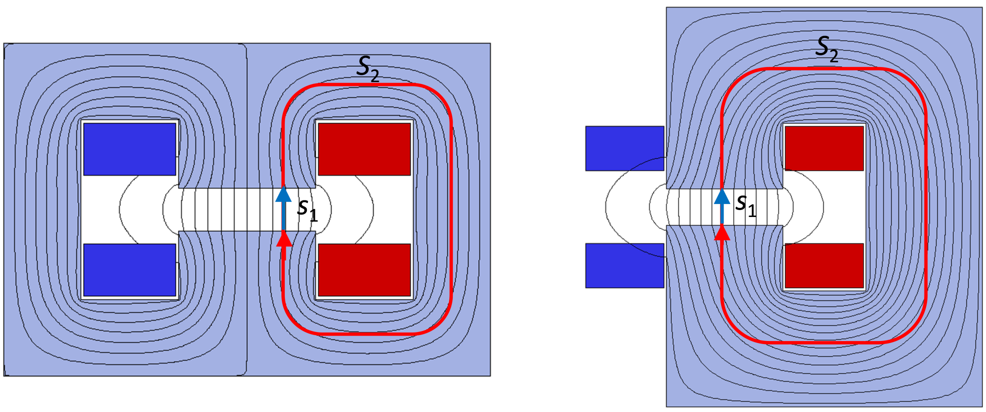

Fig. II.3.24: Closed integration path in a dipole magnet: the red line indicates the path in the iron, and the blue one indicates the path in the air gap. Left: H-shape dipole magnet. Right: C-shape dipole magnet.

In Section II.3.4.1.4, we have defined the resistance of a magnetic circuit, known as reluctance. The second term from Eq. (II.3.17)

$$\frac{\lambda_{\text{iron}}}{\mu_{\text{iron}}}$$

is called *normalized reluctance* of the yoke. It is a good practice to keep the iron yoke reluctance in the order of 10^{-2} of the air reluctance h/μ_0 through a sufficiently large iron cross section in a way that the magnetic flux in the iron remains smaller than $1.5\,\text{T}$ to avoid saturation. If the recommendation

$$\frac{\lambda_{\text{iron}}}{\mu_{\text{iron}}} < 0.01\frac{h}{\mu_0}$$

is followed diligently, the efficiency η is normally better than 99%. Now we have a definition for the efficiency η:

$$\eta = \frac{R_{\text{m,air}}}{R_{\text{m,air}} + R_{\text{m,iron}}}\,, \tag{II.3.21}$$

where $R_{\text{m,iron}}$ and $R_{\text{m,air}}$ is the reluctance of the path in iron respectively in air.

Quadrupole magnets

The excitation current in a quadrupole can be calculated by applying logic similar to that of a dipole. Choosing the integration path shown in Fig. II.3.25 we obtain

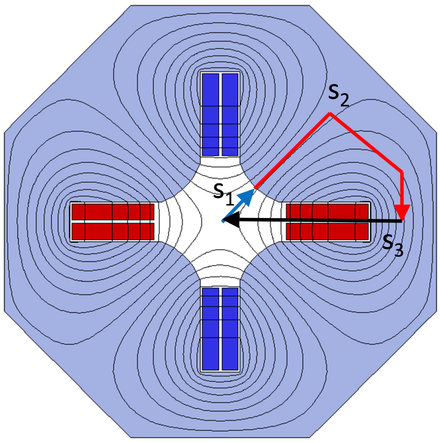

Fig. II.3.25: Closed integration path in a quadrupole magnet: the red and black lines indicate the path in the iron, and the blue one is the path in the air gap.

$$\begin{aligned} NI &= \oint \mathbf{H}\,\mathrm{ds} \\ &= \int_{s_1} \mathbf{H_1}\,\mathrm{ds} + \int_{s_2} \mathbf{H_2}\,\mathrm{ds} + \int_{s_3} \mathbf{H_3}\,\mathrm{ds}\,. \end{aligned} \tag{II.3.22}$$

For an ideal quadrupole, the gradient $B' = \frac{\mathrm{d}B}{\mathrm{d}r}$ is constant so that

$$B_x = B'y \quad \text{and} \quad B_y = B'x\,.$$

The field modulus along the path s_1 (in blue) can be hence written down as

$$H(r) = \frac{B'}{\mu_0}\sqrt{x^2+y^2} = \frac{B'}{\mu_0}r\,.$$

Assuming that μ_{iron} is large and the reluctance $R_{m,s2} = s_2/\mu_{\text{iron}}$ in the iron is small compared to the reluctance in the aperture, we can neglect H in the path s_2 (in red). Because of B_x on the x-axis being zero, the integral comes out to zero, too:

$$\int_{s_3} \mathbf{H_3}\, \mathrm{d}\mathbf{s} = 0\,.$$

As a result, we can also ignore the contribution of B along the path s_3 (in black). This leads to

$$NI \cong \int_0^r H(r)\, \mathrm{d}s = \frac{B'}{\mu_0} \int_0^r r\, \mathrm{d}s$$

and finally, to

$$NI_{(\text{per pole})} = \frac{B'\, r^2}{2\,\eta\,\mu_0}\,. \tag{II.3.23}$$

The highest magnetic field in a quadrupole is concentrated around the pole vertex. As for the dipole, we can also introduce an efficiency factor η, taking into account fringe fields and iron saturation. Interestingly, the number of ampere-turns for a given gradient increases with the square of the quadrupole aperture. The dissipated power rises even with the power of four:

$$NI \propto r^2 \quad \text{and} \quad P_\Omega \propto r^4\,.$$

This fact makes it more difficult to accommodate the required ampere-turns and coil cross section in the iron yoke and ensure adequate cooling. To make space for the coil, the hyperbola has to be truncated—at the cost of deviating from the ideal pole profile. Depending on the cut-off position, the resultant multipole errors may affect the field quality in the aperture sufficiently to warrant correction.

II.3.6.1.5 Field homogeneity

One of the simplest but most lucid ways to evaluate field quality is to plot the homogeneity of the field or of the gradient along a path, like the transversal axis or the boundary of the good-field region.

For example, the field homogeneity in a dipole can be demonstrated by plotting $\Delta B/B_0$ as shown in Fig. II.3.26. In such a plot—usually produced from results of numerical field computation or magnetic field measurements—we compare field values along the mid-plane of a magnet with the field in the centre as a reference. Achieving the following homogeneity values is reasonable but challenging:

Dipole: $$\frac{\Delta B}{B_0} = \frac{B(x,y) - B(0,0)}{B(0,0)} \leq 0.01\%$$

Quadrupole: $$\frac{\Delta B'}{B'_0} = \frac{B'(x,y) - B'(0,0)}{B'(0,0)} \leq 0.1\%$$

Sextupole: $$\frac{\Delta B''}{B''_0} = \frac{B''(x,y) - B''(0,0)}{B''(0,0)} \leq 1\%\,.$$

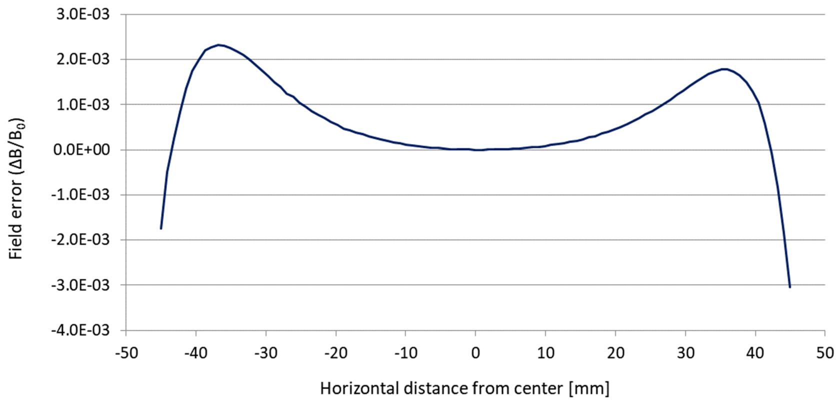

Fig. II.3.26: The transversal field error $\Delta B/B_0$ in a dipole can be plotted by comparing the field values on the x-axis (here from -45 mm to $+45$ mm) with the reference field in the centre of the magnet.

II.3.6.1.6 Pole width for dipoles

Since the uniform field region is limited to a small fraction of the pole width, we need to dimension the magnetic circuit in a way for the poles to be *wide enough* with the required field quality thus achieved within the good-field region. On the other hand, the poles should not be unnecessarily wide in order to keep the magnet compact.

To get the optimum pole width, we have several options: We can estimate the size of the poles and calculate the resulting fields numerically, but this will most probably require quite a few iterations. Experience shows that a field homogeneity $\Delta B/B_0$ in the order of 10^{-2} inside the good-field region can be achieved when

$$w_{\mathrm{GFR}} = w - h\,,$$

where w_{GFR} is a full width of the good-field region and w is a full width of the pole as shown in Fig. II.3.27. For a good-field region with

$$w_{\mathrm{GFR}} = w - 2\,h\,,$$

the field uniformity would be in the order of 10^{-3}. The aforementioned methods only allow a rough estimate. For more accurate quantification of the field quality, in particular, when we search for a homogeneity better than 10^{-3}, we either employ numerical simulations or make use of an empirical formula proposed in [5] to calculate the necessary pole width analytically:

$$x_p = \frac{h}{2} f\left(\frac{\Delta B}{B_0}\right)\,, \tag{II.3.24}$$

where x_p is the pole overhang or excess of the pole beyond the edge of the good-field region, as indicated in Fig. II.3.27. The width of the poles with respect to the good-field region depends ultimately on the aperture height and the field uniformity either in the 10^{-2}, 10^{-3} or 10^{-4} range. In the case of an unoptimised pole contour of a dipole, which means the pole is flat all the way to the pole edge, the required pole width can be computed with:

$$f\left(\frac{\Delta B}{B_0}\right)_{\text{unopt.}} = -0.36\ln\frac{\Delta B}{B_0} - 0.90\,. \tag{II.3.25}$$

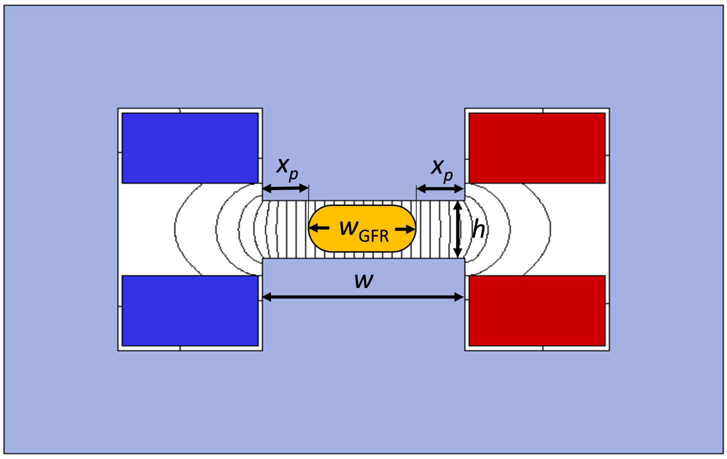

Fig. II.3.27: The pole width needs to be extended beyond the good-field region such that the required field quality can be achieved within the good-field region.

II.3.6.1.7 Pole optimisation

Along with the unoptimised poles, we also need to discuss their opposites—optimised poles. The field quality in the good-field region can be improved either by increasing the pole width, a trivial but disadvantageous method that accounts for a significant increase in a magnet's size and mass, or by optimising the pole profile.

An optimised pole is a pole with the edges adjusted by different methods to improve the field homogeneity in the good-field region without increasing the pole width. A commonly used method to achieve this is designing little bumps and dents at the pole edges—called shims. The shims can be seen as pieces of ferromagnetic material added on each side of the poles to compensate for the cut-off of the ideal pole. The area and shape of the shims determine the amplitude of multipole errors. An additional way to ameliorate the field quality involves tapering or rounding off the pole edges, thus minimising their saturation. Figure II.3.28 compares an unoptimised pole contour (left) of a dipole with an optimised pole profile featuring a shim and a chamfered edge.

Should we intend to optimise the pole profile in any way, we can make use of our empirical formula, tailoring it accordingly for an optimised pole:

$$f\left(\frac{\Delta B}{B_0}\right)_{\text{opt.}} = -0.14\ln\frac{\Delta B}{B_0} - 0.25\,. \tag{II.3.26}$$

A successful application of Eq. (II.3.26) to reduce the pole overhang depends mainly on the efforts in the pole optimisation process. A similar approach exists for quadrupoles.

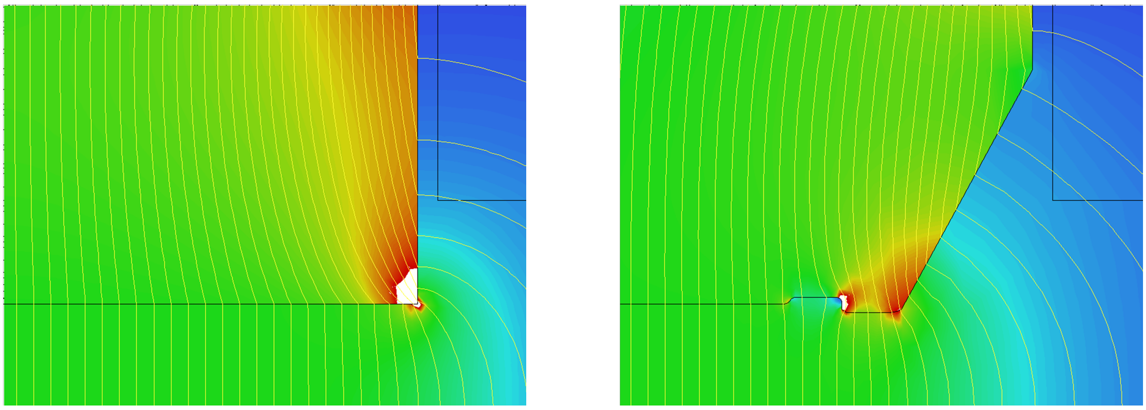

Fig. II.3.28: Pole edge contours on a dipole. Left: unoptimised contour with flat pole and straight cut-off. Right: optimised contour with shim and tapered cut-off to reduce saturation on the pole edge.

II.3.6.1.8 Yoke dimensioning

Having calculated and optimised the pole width, we can now dimension the rest of the magnetic circuit. In Section II.3.4.1.4, we highlighted the necessity of avoiding saturated areas in the yoke. In order to identify any saturation issue in the iron, we need to estimate the average flux density in the individual parts of the yoke. Rather than immediately running a computer simulation, it is much easier to make a first-order approach on paper using the concept of magnetic flux:

$$\Phi = \int_{a_m} B_\perp \, \mathrm{d}a \ . \tag{II.3.27}$$

We should keep in mind that the term magnetic flux Φ through a surface is defined as the surface integral of the normal component of the total flux density passing through the cross section of this surface. If we assume that there is no significant stray flux outside the iron and the flux in the iron circuit remains more or less constant, the total flux Φ_f in the return yoke must be equal to the flux Φ_F in the air gap (see Fig. II.3.29 left).

This flux Φ_F includes the flux from the aperture and the stray flux outside the aperture. The stray flux extends approximately one aperture height on either side of the aperture, so the total flux from the air gap is approximately

$$\Phi_F \cong B\,(w + 2h)\, l_{\text{eff}} \ , \tag{II.3.28}$$

where B is the flux density in the aperture, and l_{eff} is the effective magnetic length (we will define this term in the next section). Applying the principle of flux conservation, we can now estimate the flux density B_{leg} in any part of the yoke using

$$B_{\text{leg}} \cong B \frac{w + 2h}{w_{\text{leg}}} \ , \tag{II.3.29}$$

where w_{leg} is the width of a corresponding section in the yoke as shown in Fig. II.3.29 (right). With this simple approximation, we can make a final check on whether all parts remain within the limits of

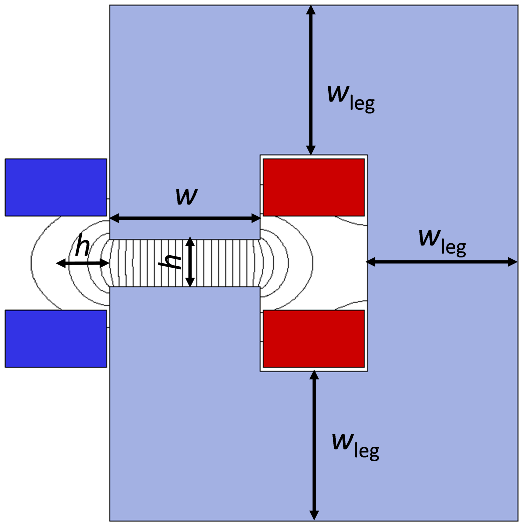

Fig. II.3.29: Constant flux in a magnetic circuit. Left: The flux in the iron yoke must equal the flux in the aperture. Right: The flux in the aperture also includes the stray flux.

saturation. If one part turns out to be saturated, we need to adjust the width of this section so that it no longer reaches the saturation limit.

II.3.6.1.9 Effective magnetic length

In the context of magnet design, we will frequently make use of the essential but often misinterpreted term *effective magnetic length*, sometimes also referred to as *effective length* or *magnetic length*.

To understand the concept of magnetic length, we should look at the schematic representation of a dipole magnet in Fig. II.3.30. Let us imagine approaching the magnet in longitudinal z-direction with a measurement probe along the beam axis from infinity towards the magnet centre. What we should read on the instrument is a steady increase in the magnetic flux density when moving closer to the edge of the iron yoke through the stray field of the magnet.

The field should continue to rise even in the aperture of the magnet, reaching its maximum value B_0 towards the centre of the magnet, where it should remain stable. The field should decrease again away from the centre towards the other end of the magnet and beyond the magnet to infinity, where the field should finally be zero.

Integrating the magnetic field along the longitudinal axis, starting from far outside on one side and ending far outside on the other side, gives a higher value than simply multiplying the central magnetic field with the yoke length of a magnet. Here, we can introduce the term *effective magnetic length* expressed by

$$l_{\mathrm{eff}} = \frac{\int_{-\infty}^{\infty} B(z)\,\mathrm{d}z}{B_0}\,. \tag{II.3.30}$$

The effective magnetic length l_{eff} is defined as the magnetic field integrated along the longitudinal

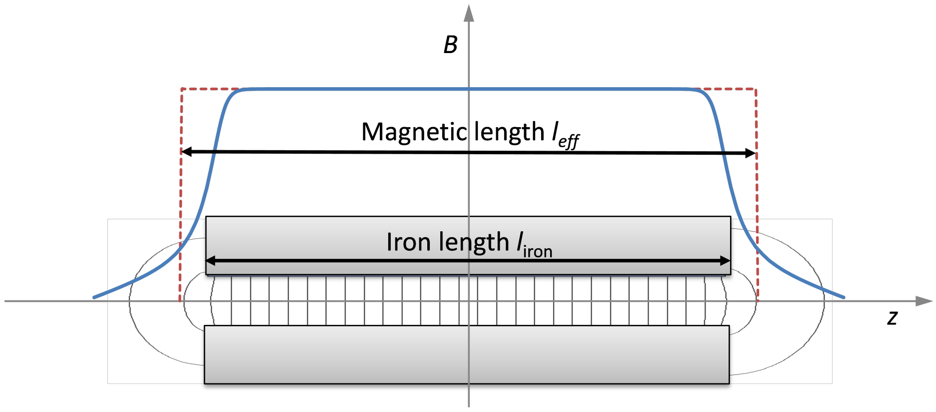

Fig. II.3.30: Poles of a dipole magnet with flux lines: the true field shape is represented by the blue curve with its maximum value B_0 at the centre of the magnet; the red dashed line represents the hard-edge model with the effective magnetic length.

axis of the magnet divided by the central field value B_0. When calculating the integrated magnetic field from the central field, we should not confuse the magnetic length l_{eff} and the yoke length l_{yoke}. The magnetic length l_{eff} must be used:

$$\int_{-\infty}^{\infty} B(z)\,\mathrm{d}z = B_0\, l_{\text{eff}}\,. \tag{II.3.31}$$

The hard-edge model, as shown in Fig. II.3.30 (red dashed line), is often used to represent a magnet in beam-optic codes. This model uses the central field B_0 of a magnet and its effective length. Contrary to a real magnet, where the field fades out at the upstream and downstream edge of the magnet, the field in the hard-edge model changes abruptly from $B = B_0$ to $B = 0$.

We can conclude that the magnetic length is always longer than the yoke length. The magnetic length depends on several factors: the existence of saturated regions, the shape of the coil ends, and the shape of the pole ends in the longitudinal direction. The exact magnetic length can be determined by magnetic measurements or 3D numerical simulations.

For our analytical design, though, it is possible to estimate roughly the magnetic length by this simple relation

$$l_{\text{eff}} \cong l_{\text{yoke}} + h\,. \tag{II.3.32}$$

This estimation works only for long magnets, where the longitudinal dimension is much larger than the aperture. On the other hand, a 3D computation is compulsory for short magnets to find the magnetic length.

The concept of magnetic length holds equally for quadrupoles by substituting the flux density B with the gradient G. The magnetic length for a long quadrupole can be approximated with

$$l_{\text{eff}} \cong l_{\text{yoke}} + 2h/3\,. \tag{II.3.33}$$

II.3.6.1.10 Sagitta

In Section II.3.6.1.3, we have seen that the centre of the good-field region is determined by the position of the central orbit of the particle beam. This means that the good-field region must follow the theoretical beam trajectory through all the magnets in our accelerator or beamline. For a curved dipole, the poles follow more or less the curve of the beam trajectory, and so does the good-field region. The pole overhang to the left and right from the good-field region remains constant, as we can see in Fig. II.3.31 (left).

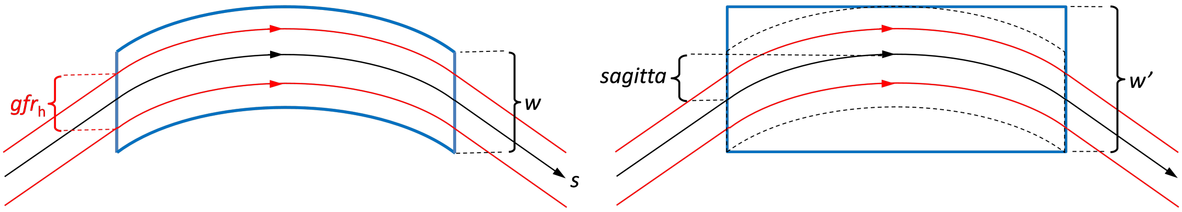

Fig. II.3.31: Horizontal good-field region (top view on the pole). Left: curved dipole magnet. Right: straight dipole magnet with sagitta.

What happens if we consider designing a straight magnet with rectangular poles that do not follow the beam trajectory? If we theoretically take the same pole width as in the case of a curved magnet, the size of the pole overhang would change along the magnet because the good-field region still had to follow the curved beam trajectory. This would have a negative impact on the field quality in the good-field region. Therefore, we need to enlarge the width of the rectangular poles to correctly accommodate the curved good-field region as shown in Fig. II.3.31 (right). The transversal excursion of the beam when travelling through a straight magnet is called sagitta S and can be calculated by using

$$S = r_m \left(1 - \cos\left(\frac{\Theta}{2}\right)\right)\,, \tag{II.3.34}$$

where r_m is the bending radius of the beam trajectory and Θ is the bending angle of the magnet. The new enlarged pole width w' is then

$$w' = w + S\,. \tag{II.3.35}$$

II.3.6.2 Coil design

Coils are a fundamental part of electromagnets: They generate the magnetomotive force necessary to produce the required flux density in the magnet aperture. We will dedicate the following section to explaining the basic principles of coil design.

In the previous section, we saw how to calculate the ampere-turns necessary to create a magnetic field. In this part, we will discuss how to define an appropriate current density, how to divide the ampere-turns into current and number of turns in a sensible way, and how to find a good coil cross section.

II.3.6.2.1 Coil cross section

The previously determined ampere-turns NI have now to be divided into the number of conductor turns N_T and current I within one conductor turn. While keeping the ampere-turns constant, we can either choose a large number of turns and a low current (Fig. II.3.32 left) or opt for a small number of turns and a high current (Fig. II.3.32 right) or go for something in-between. Before deciding the number of turns, it is good to know some fundamental relations as presented in Table II.3.4.

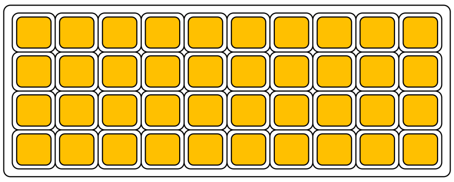

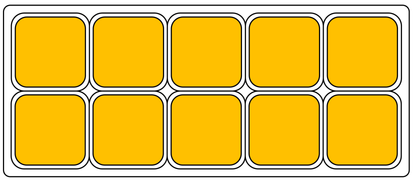

Fig. II.3.32: Different coil layouts for the same ampere-turns. Left: a large number of turns combined with low current. Right: a small number of turns with high current.

Table II.3.4: Design parameters depending on the number of turns in the excitation coils.

Large N_T = low current = high voltage	Small N_T = high current = low voltage
Small terminals	Large terminals
Small conductor cross section	Large conductor cross section
Thick insulation for coils and cables	Thin insulation in coils and cables
Less good filling factor in the coils	Good filling factor in the coils
Low power transmission loss	High power transmission loss

Many turns imply low current but high voltage, which consequently requires thicker insulation for both coils and cables. Among the positive effects, we count low transmission power losses even across long distances between the power converter and the magnets. Therefore, the choice for coils with many turns is primarily for magnets with moderate magnetic field strength powered individually.

On the other hand, a small number of turns means high current but low voltage. However, there are some drawbacks to note: bulky terminals and large conductor cross section. Among the advantages are less stringent demands on the insulation of conductors and cables. Due to high transmission power losses, we only opt for this solution when many magnets have to be electrically connected in series with a relatively short distance, like in the example of bending magnets in a synchrotron. In this case, coils with many turns would lead to an unreasonably high voltage between the coils and the magnet yokes, increasing the risk of short circuits. The higher transmission power loss can be handled using water-cooled cables or rigid bus bars with large cross sections.

In some instances, the coil layout depends on the topology of an existing power converter design. This means that either the maximum current of the converter determines the current in coils and, therefore, the number of turns, or in cases of cycled or pulsed magnets, the coil inductance limits the number of turns, and the coil current has to be adjusted accordingly. A large number of turns means a high inductance and requires a high voltage to drive a certain change rate in current $\frac{\mathrm{d}I}{\mathrm{d}t}$.

When the maximum current available from the converter $I_{\max}$ dictates the current in the coils, it is a good practice to include a safety margin, typically 10%, between the two parameters to compensate for possible imprecision during the design, manufacturing, or operation.

The decision on the number of turns has only a minor impact on the size of the coil as long as the current density does not change. For coils with many turns, the insulation thickness needs to be increased to cope with higher voltage. This results in a lower conductor filling factor in the coil leading to a slightly larger coil cross section compared to coils with fewer turns.

II.3.6.2.2 Current density

Our next step will be to find a suitable value for the current density. The current density J $[J] = 1\,\mathrm{A\,m^{-2}}$ is defined by

$$J = \frac{I}{a_c}\,, \tag{II.3.36}$$

where a_c is the *net* conductor cross section $[a_c] = 1\,\mathrm{m^2}$, including only the part of the conductor made of any conducting material, but not the insulation or the cooling duct. The current density is an essential parameter because, for a given magnetic field and magnet geometry, the total power loss in a magnet is directly proportional to the current density. We can observe this in the following relations that describe the power dissipated in a dipole, quadrupole, and sextupole, respectively:

$$P_{\Omega,\mathrm{dip}} = \rho_e \frac{B\,h}{\eta\mu_0} J\,l_{\mathrm{avg}}\,, \tag{II.3.37}$$

$$P_{\Omega,\mathrm{quad}} = 2\rho_e \frac{B'\,r^2}{\eta\mu_0} J\,l_{\mathrm{avg}}\,, \tag{II.3.38}$$

$$P_{\Omega,\mathrm{sext}} = \rho_e \frac{B''\,r^3}{\eta\mu_0} J\,l_{\mathrm{avg}}\,, \tag{II.3.39}$$

with l_{avg} being the average length of one conductor turn $[l_{\mathrm{avg}}] = 1\,\mathrm{m}$ and ρ_e the conductor resistivity. Without knowing the average length of the conductor yet, we do not use the Eqs. (II.3.37), (II.3.38), or (II.3.39) for accurate power calculations. They are mentioned here only to illustrate the strict proportionality of the selected current density to the dissipated power in a magnet.

In addition, the current density directly impacts the coil size, the coil cooling, the choice of power converter, the investment and operating costs. A low current density means lower power consumption but a larger coil and consequently a larger magnet cross section. Thus a low current density implies lower operating costs but a higher capital investment due to higher material costs.

As mentioned above, the current density defines the type of cooling. A conservative upper limit for water-cooled coils is $10\,\mathrm{A\,mm^{-2}}$ and not much more than $1.5\,\mathrm{A\,mm^{-2}}$ for air cooling with natural convection. We will discuss it more extensively in Section II.3.6.3.

Additional constraints related to the maximum capacity of the power converter in terms of current, voltage, and power might exist. If the parameters of the power converter are already fixed, we need to design a magnet matching these particular requirements. This restriction might, therefore, also limit the current density. It becomes apparent that a sensible choice of the current density is crucial for a robust and economical magnet design.

II.3.6.2.3 Electrical parameters

Besides the current density, we need to define and compute other electrical quantities, such as the resistance of a coil, voltage drop along a coil, and dissipated power. As we can see here, the current density also has a direct impact on these electrical parameters:

$$R \propto N_T^2 J \qquad U \propto N_T J \qquad P_\Omega \propto J\,.$$

The coil resistance R is proportional to the current density and to the square of the number of turns in a coil; the voltage drop U is proportional to the current density and the number of turns; the power P_Ω is proportional just to the current density. Here, we will recall a few fundamental relations.

The resistance R of a coil is defined as

$$R = \frac{N_T l_{\text{avg}}}{a_c \sigma_e}\,, \tag{II.3.40}$$

where σ_e is the electrical conductivity, the reciprocal value of the resistivity ρ_e, of the conductor material. We must know that the electrical conductivity is temperature dependent: The coil resistance changes with temperature. To obtain the accurate resistance value for the cooling parameters under operating conditions, we have to correct the resistance at room temperature for the assumed operation temperature by using

$$R(T) = R(T_0)\left(1 + \alpha\left(T_{\text{avg}} - T_0\right)\right)\,, \tag{II.3.41}$$

where T_0 is the room temperature of 20° C, T_{avg} is the average temperature of the conductor in operation, and α is the temperature coefficient of the resistivity of the conductor material. Later in Section II.3.6.3 dedicated to water cooling of coils, we will introduce the terms T_{in} and T_{out}, which are the temperatures of the coil at the cooling water inlet and outlet, respectively. The average temperature of the conductor can then be calculated with

$$T_{\text{avg}} = \frac{T_{\text{in}} + T_{out}}{2}\,. \tag{II.3.42}$$

Ohm's law relates the static voltage across an electrical circuit with the current in the circuit via the resistance of the circuit:

$$U = RI\,. \tag{II.3.43}$$

The ohmic power dissipated in this electrical circuit is

$$P_\Omega = UI = RI^2\,. \tag{II.3.44}$$

For circuits not operated with a constant current, the effective current has to be used instead.

II.3.6.3 Coil cooling

The heat dissipated due to power losses must be removed from the coils to prevent overheating that can seriously damage the coil insulation and cause short circuits between the coil conductor and surrounding equipment. In the field of normal-conducting magnets, we distinguish between two different cooling techniques: *air cooling* and *water cooling*. They are sometimes referred to as *dry cooling* and *wet cooling*.

For slowly cycled magnets or those operated at constant current, it is usually sufficient to consider only ohmic losses when designing a cooling circuit. In the case of fast-pulsed magnets, additional power losses occur both in the coils and yokes due to induced eddy currents. These specific cases will not be discussed here.

II.3.6.3.1 Air cooling

Air cooling by natural convection is suitable only for low current densities. This limits the application to magnets with moderate field strength, like corrector or steering magnets. As a rule of thumb, the maximum current density for voluminous coils, which are almost entirely enclosed in the magnet yoke, should not exceed $1\,\mathrm{A\,mm^{-2}}$. For small, thin coils, as shown in Fig. II.3.33 (left), the current density can be higher but should remain below $2\,\mathrm{A\,mm^{-2}}$.

A precise thermal study of air-cooled coils by analytical means proves to be difficult, if not impossible. Air cooling, a combination of convection, radiation, and heat conduction, depends on factors such as coil geometry, coil surface characteristics (roughness, material, colour), thermal contact with the surrounding materials, etc. Should we need a detailed analysis of the thermal behaviour, numerical computations (see Fig. II.3.33 right) or measurements will be required. Information on air cooling and cooling in general can be found in subject-related literature [6].

Air-cooled coils are typically made of round, rectangular or square wires. These conductors are commercially available in various grades and dimensions. They can be ordered blank or pre-impregnated with varnish ($0.02 \leqslant$ thickness $\leqslant 0.1\,\mathrm{mm}$) or wrapped in polyimide (Kapton®®) tape ($0.1 \leqslant$ thickness $\leqslant 0.2\,\mathrm{mm}$). Depending on the winding precision, insulation thickness, and conductor cross section, we can obtain a coil filling factor f_c between 0.63 (round conductor) to 0.8 (rectangular conductor). The outer or ground insulation typically comprises epoxy-impregnated glass-fibre tapes between 0.4 and $2.0\,\mathrm{mm}$ thick. In specific cases, the cooling performance of air-cooled coils can be slightly enhanced by mounting an appropriate heat sink with an enlarged radiation surface or by using forced airflow (cooling fan).

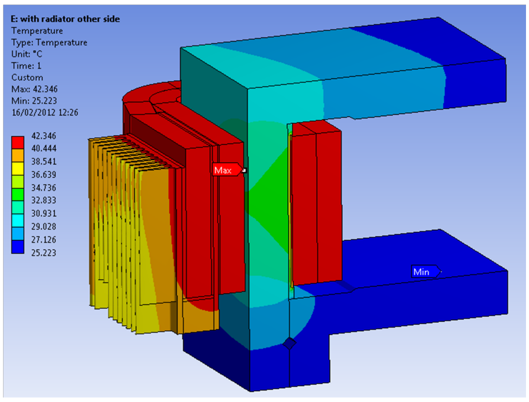

Fig. II.3.33: Air-cooled coils. Left: thin air-cooled coil suitable for current densities up to $2\,\mathrm{A\,mm^{-2}}$. Right: a thermal finite-element model of an air-cooled coil with an additional heat sink.

II.3.6.3.2 Water cooling

There are two types of water cooling: *direct* and *indirect* water cooling. Of minor importance and rarely used, the latter has the advantage of not requiring cooling plants with water treatment for demineralized water—normal tap water serves as a coolant. As illustrated in Fig. II.3.34 (left), the method, as mentioned above, implies a more complex coil design. When air cooling reaches its maximum capacity, mounting an external heat sink cooled with tap water can enhance the cooling performance by keeping the thermal load within limits or permitting slightly higher current densities. With indirect cooling hardly used, we will focus here on the engineering and construction of directly water-cooled coils.

The current density in a directly water-cooled coil can typically be as high as $10\,\mathrm{A\,mm^{-2}}$. This conservative value can be easily obtained with standard coil layouts. Higher current densities would necessitate a sophisticated cooling circuit design with multiple parallel circuits in each coil and high coolant velocity, which would increase the risk of erosion.

Standard water-cooled coils are made of copper or aluminium conductor with a rectangular or square cross section and a central cooling duct for demineralized water, as shown in Fig. II.3.34 (right). The interturn and the ground insulation consist of one or more layers of half-lapped glass-fiber tape impregnated in epoxy resin. The interturn insulation thickness lies typically between 0.3 and $1.0\,\mathrm{mm}$, the ground insulation should be between 0.5 and $3.0\,\mathrm{mm}$ depending on the applied voltage.

II.3.6.3.3 Cooling parameters

Water cooling is necessary when we have to handle higher current densities and want to avoid larger coil cross sections. The construction of water-cooled coils requires hollow conductors with a cooling channel. Choosing the correct parameters and dimensions—such as the number of cooling circuits, size of the cooling channel, and flow rate—is not easy, and it takes several iterations to arrive at a satisfactory solution. This section addresses the calculation and design of an efficient cooling circuit.

Before entering the subject, there are a few recommendations and general rules that should help us make adequate choices. It is essential to remember that these are rules of thumb and should be scrutinised as to their validity and applicability in a particular situation.

As already mentioned, the current densities for water-cooled coils should be kept between

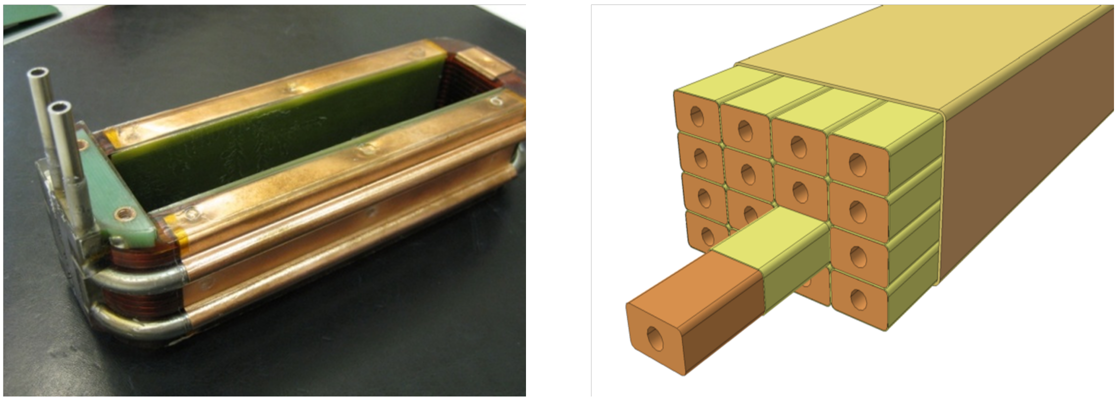

Fig. II.3.34: Water-cooled coils. Left: coil with indirect water cooling. The heat is transferred from the conductor through the insulation to the cooling circuit, which removes it using regular tap water. Right: coil with direct water cooling. Demineralized water is circulating in the conductor's central cooling duct, removing the heat dissipated in the conductor.

2 and $10\,\mathrm{A\,mm^{-2}}$. Below these values, air cooling is usually sufficient; exceeding this threshold implies more complex and, thus, costly cooling layouts.

The pressure typically provided by modern cooling plants ranges between 0.1 and 1.0 MPa, which corresponds to 1.0 and 10 bar receptively. Advanced cooling stations can supply water with a pressure up to 2.0 MPa (20 bar). Low water pressure can be compensated to a certain extent by a higher cooling flow rate as well as by a sophisticated and, hence, expensive coil design with several cooling circuits in parallel.

The velocity of the cooling medium—in general, demineralized water—should be sufficiently high to guarantee a turbulent flow but low enough to avoid erosion and vibration. With the absolute limit usually fixed at $4\,\mathrm{m\,s^{-1}}$, in more conservative and reliable designs, the value shall remain below $3\,\mathrm{m\,s^{-1}}$.

To reduce or avoid accelerated ageing of insulation materials, particularly in the presence of ionizing radiation, it is advisable to specify the temperature of coil surfaces at 60°C maximum. This upper limit, together with an inlet water temperature of less than 30°C leads to a maximum water temperature rise of 30°C in the coils, keeping the thermal stress under control.

Some applications require high mechanical stability and, consequently, good thermal stability. In such cases, the maximum temperature rise has to be reduced accordingly. For synchrotron light sources and medical accelerators, target values of 15°C temperature increase are frequently quoted. The formulas in the next section are valid under the following assumptions:

- the cooling pipes are always long, mostly straight and smooth inside without perturbations in the cross section;
- the flow is turbulent, which suggests a high Reynolds number;
- a good heat transfer from conductor to coolant, with the temperature of the inner surface of the conductor equal to that of the coolant;
- the conductor is isotherm over its cross section;
- the entire joule heating is removed by the coolant fluid;

– the contribution from the air convection is negligibly small: In practice, the fraction of heat removed by natural convection being only in the order of few percent.

II.3.6.3.4 Heat transfer basics

The topic of heat transfer is pretty comprehensive and fills many pages of fluid mechanics and thermodynamics textbooks like [6]. As it is not within the scope of this chapter to treat the related aspects in detail, we will restrict ourselves to a few crucial laws and expressions regarded as beneficial for the basic understanding and design of cooling circuits for magnets.

Heat evacuation by a coolant fluid can be described by the heat balance equation

$$\frac{\mathrm{d}W}{\mathrm{d}t} = Q\delta c_p \Delta T\,, \tag{II.3.45}$$

where W is the heat or the thermal energy, Q is the flow rate of the coolant, δ is the mass density of the coolant, c_p is the heat capacity of the coolant, and ΔT is the temperature difference between the cooling water outlet temperature T_{out} and the inlet temperature T_{in}. If we consider a hollow conductor, which is constantly heated by the ohmic losses P_Ω, and we further assume that the heat flow from the inner conductor surface to the coolant is constant, we can reformulate Eq. (II.3.45) to

$$Q = \frac{P_\Omega}{\delta c_p \Delta T}\,, \tag{II.3.46}$$

which defines now the coolant flow rate Q necessary to remove the electrical power P_Ω dissipated in the conductor material while keeping the temperature rise ΔT constant.

Having found an expression to calculate the cooling flow rate, the next step is to derive all other cooling parameters: the pressure loss, coolant velocity, and dimensions of the cooling circuit. A good starting point is to take the Darcy–Weisbach equation—an empirical equation that relates the pressure drop due to friction along a given pipe length to the average fluid velocity:

$$\Delta P = f_h \frac{l_h}{d_h} \frac{\delta v_{\mathrm{avg}}^2}{2}\,. \tag{II.3.47}$$

In this equation, ΔP is the pressure loss, f_h is a unit-less friction factor, l_h is the length of the cooling pipe, d_h is the equivalent hydraulic diameter of the cooling pipe, and v_{avg} is the average coolant velocity. For pipes with noncircular cooling ducts, the equivalent hydraulic diameter can be determined with

$$d_h = f_h \frac{4\,a_h}{s_h}\,, \tag{II.3.48}$$

where a_h is the area of the cooling duct cross section and s_h the *wetted* perimeter of the cooling duct; for a circular pipe the hydraulic diameter $d_h = d$.

The friction factor f_h depends on the Reynolds number Re, which relates the inertial and viscous forces in a fluid problem:

$$Re = \frac{v_{\text{avg}} d_h}{\nu}\,, \tag{II.3.49}$$

with ν describing the temperature-dependent kinematic viscosity of a coolant. The Reynolds number helps predict the flow pattern in a fluid under different conditions: It indicates whether a flow is laminar, turbulent or in the transition regime. A flow with the Reynolds number below 2100 is always laminar. In some cases, the flow can remain laminar up to $Re = 10\,000$. In the transition regime, where the Reynolds number is between 2300 and 4000, the flow is neither fully laminar nor fully turbulent. For a flow to be thermally effective, it should be in the turbulent range. In our application context, we assume that a flow is in the moderate turbulent regime if $4000 \leqslant Re \leqslant 100\,000$.

Erosion phenomena occur above the upper limit of $Re = 100\,000$, so we should avoid going beyond this limit.

The friction factor is also a function of the relative roughness of the cooling duct. There are several formulas aimed at defining the friction factor for different flow conditions. Most of them are included in the Moody diagram [7], which relates the friction factor, Reynolds number, and surface roughness for a fully developed flow in a circular pipe. The accuracy of these formulas is in the order of $\pm 5\%$ for smooth pipes and $\pm 10\%$ for rough pipes—usually sufficient for all practical purposes.

For a purely laminar flow, the friction factor is

$$f_h = \frac{64}{Re}\,. \tag{II.3.50}$$

Whereas for our application, where the flow needs to be turbulent, the relationship between the friction factor, Reynolds number, and relative roughness is more complex. The Colebrook-White equation for turbulent flow serves as a model for this relationship:

$$\frac{1}{f_h} = -2\log_{10}\left(\frac{\varepsilon}{3.7\,d_h} + \frac{2.51}{Re\sqrt{f_h}}\right)\,. \tag{II.3.51}$$

Due to its implicit nature, this equation normally needs to be solved iteratively for the friction factor. The Blasius equation is an approximation of the Colebrook-White Eq. (II.3.51):

$$f_h = \frac{0.3164}{\sqrt[4]{Re}}\,. \tag{II.3.52}$$

Not including a term for the pipe roughness, this Eq. (II.3.52) represents a much simpler approach for computing the friction factor. This model is valid only for smooth pipes and the Reynolds number of up to $100\,000$. Inserting Eq. (II.3.52) into Eq. (II.3.47) and reformulating it to express v_{avg}, we obtain

$$v_{\text{avg}}^2 = \frac{2\,\Delta P}{\delta}\frac{d_h}{l_h}\frac{1}{0.3164}\sqrt[4]{\frac{v_{\text{avg}} d_h}{\nu}}\,, \tag{II.3.53}$$

which allows us to calculate the coolant velocity as a function of the pressure drop and the cooling hole diameter in the conductor.

II.3.6.3.5 Cooling circuit design

In the previous section, we derived the formulas required to calculate the main parameters of a cooling circuit. Finding a good solution for a cooling layout is an iterative and sometimes lengthy process, and different methods lead to a satisfactory design. In the following paragraphs, we will share a well-established method of designing a cooling circuit.

For this specific section, we will make an exception. Instead of SI units we will use more practical units for $[Q] = 1\,\mathrm{L\,min^{-1}}$ (litre per minute) for the flow rate, $[P] = 1$ bar for the pressure, $[P_\Omega] = 1\,\mathrm{kW}$ for the dissipated power, and $[d_h] = 1$ mm for the hydraulic diameter. For all other parameters, we will continue to use SI units.

First, we want to translate some of the equations from the previous section into a more compact expression. Using water as a cooling medium, we introduce the values for the density $\delta = 993\,\mathrm{kg\,m^{-3}}$, the kinematic viscosity $\nu = 6.982 \times 10^{-7}\,\mathrm{m^2\,s^{-1}}$ and the specific heat capacity $c_p = 4.18\,\mathrm{kJ\,kg^{-1}\,K^{-1}}$ of water at 310 K.

Therefore we can simplify the Eq. (II.3.46) to

$$Q = 14.5\,\frac{P_\Omega}{\Delta T}\,, \tag{II.3.54}$$

where Q is now the flow rate in $L\,\mathrm{min}^{-1}$. To increase the temperature of 1 kg of water by 1 K, we need an energy of 1 kcal corresponding to 4.186 kJ. By increasing its temperature by 1 K, a water flow of $1\,\mathrm{L\,s^{-1}}$ can consequently evacuate 4.186 kW. As a rule of thumb, for a temperature rise of $\Delta T = 30$ K, every litre per minute can cool approximately 2 kW of dissipated power. Next, we will reduce Eq. (II.3.53) to

$$v_{\mathrm{avg}} = 2.188\,d_h^{5/7}\left(\frac{\Delta P}{l_h}\right)^{4/7}\,. \tag{II.3.55}$$

For a turbulent flow characterized by a Reynolds number larger than 4000, we define the minimum average water velocity:

$$v_{\mathrm{avg,min}} = \frac{4000}{d_h}\nu \cong \frac{2.8}{d_h}\,. \tag{II.3.56}$$

When rewriting Eq. (II.3.47), we can find an expression for the pressure loss:

$$\Delta P = 0.254\,\frac{v_{\mathrm{avg}}^{1.75}}{d_h^{1.25}}\,l_h\,. \tag{II.3.57}$$

By using

$$v_{\mathrm{avg}} = 16.67\,\frac{Q}{d_h} = 66.67\,\frac{Q}{d_h^2\pi}\,, \tag{II.3.58}$$

Equation (II.3.57) becomes

$$\Delta P = 53.32\,\frac{Q^{1.75}}{d_h^{4.25}}\,l_h\,, \tag{II.3.59}$$

which allows us to determine the required pressure loss for a given flow rate and hydraulic diameter. However, we often know the required flow rate and the limitations of our cooling system in terms of available pressure. In this case, it can be advantageous to reformulate Eq. (II.3.59) again so that we can find the required hydraulic diameter from a given flow rate and an assumed pressure drop:

$$d_h = 2.31\, Q^{0.368} \left(\frac{l_h}{\Delta P}\right)^{0.21} . \tag{II.3.60}$$

Finally, if we want to use millimetre as a unit for the hydraulic diameter d_h to calculate the Reynolds number Re, we need to adapt Eq. (II.3.49) accordingly:

$$Re = \frac{v_{\text{avg}} d_h}{\nu}\, 10^{-3} . \tag{II.3.61}$$

In general, we start the design of our cooling system with the assumption that we have one single cooling circuit per coil. In this case, the hydraulic length is equal to the total length of the conductor, and the connection hoses or tubes can be neglected because they are short compared to the cooling circuit.

Coils with elevated current densities and power losses require high coolant flow rates, which might not be achievable with a single cooling circuit because the upper limit for parameters like pressure drop and coolant velocity would be quickly reached. To remedy this problem, we need to divide the coil cooling into two or more parallel cooling circuits. Introducing K_h as the number of water circuits per coil, we can use the new terms Q' and l'_h in our usual Eqs. (II.3.55), (II.3.59), and (II.3.60) to calculate the cooling parameters for a coil with more than one cooling circuit:

$$Q' = \frac{Q}{K_h} \qquad l'_h = \frac{l_h}{K_h} .$$

From Eq. (II.3.59), we can easily find out that the pressure drop is inversely proportional to approximately the third (precisely: 2.75^{th}) power of the number of cooling circuits K_h per coil:

$$\Delta P \propto \frac{1}{K_h^{2.75}} . \tag{II.3.62}$$

This implies that for a given flow the pressure drop is reduced by almost a factor of eight when doubling the number of circuits.

Another relation is of interest as it affects the cooling performance even more and thus should be considered in the system layout. The pressure drop is inversely proportional to approximately the fifth (exactly: 4.75^{th}) power of the cooling channel diameter:

$$\Delta P \propto \frac{1}{d_h^{4.75}} . \tag{II.3.63}$$

This implies that an increase in the cooling channel diameter by a small fraction can reduce the required pressure drop significantly. Let us now establish a general procedure to derive step-by-step all required cooling parameters:

1. We calculate the conductor net cross section from the current density and the current.

2. From the number of turns and the average turn length, we can compute the coil resistance.

3. We define the allowed temperature rise and correct the coil resistance for the average conductor temperature according to Eqs. (II.3.41) and (II.3.42) before computing the ohmic losses in the coil.

4. With Eq. (II.3.54), we can calculate the required flow rate of water to evacuate the total ohmic losses from the coil by keeping the temperature increase within the defined limit.

5. For a given cooling duct diameter and flow rate, we can determine the pressure loss with Eq. (II.3.59). Alternatively, we can use Eq. (II.3.60) to calculate the diameter of the cooling duct from a given flow rate and pressure drop.

6. If necessary, we can change the pressure drop, the hydraulic diameter or the number of cooling circuits per coil and iterate over point 5.

7. We check that the coolant velocity remains below the limit, where erosion phenomena become apparent.

8. Finally, we need to verify that the Reynolds number is in the turbulent flow regime, for which the Blasius equation holds. The Reynolds number should be between 4000 and $100\,000$.

The attentive reader might find some differences when comparing the formulas in this chapter with those in textbooks; these discrepancies can be explained by the temperature dependence of some material constants, which is sometimes neglected in the case of simplified formulas.

Exercises

Exercise 1: Right-hand rule

A proton enters the magnet in Fig. II.3.35 in the positive z-direction. A magnetic dipolar field points in the negative y-direction. With the help of the right-hand rule, find out in which direction the particle will be deflected (positive or negative x-direction).

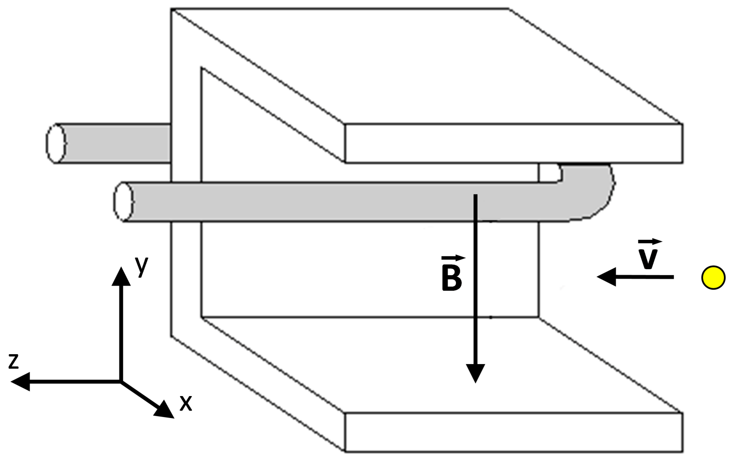

Fig. II.3.35: Exercise 1 - Application of right-hand rule.

Exercise 2: Beam rigidity

For a synchrotron, 16 bending magnets are required. The synchrotron accelerates the protons to the energy between $60\,\mathrm{MeV}$ and $220\,\mathrm{MeV}$ and the fully-stripped carbon ions C^{6+} to the energy between $120\,\mathrm{MeV/u}$ and $400\,\mathrm{MeV/u}$. The injection energy for both particle types is $7\,\mathrm{MeV/u}$.

For which operation range (minimum and maximum beam energy) do the magnets have to be designed? Calculate the corresponding beam rigidity.

Exercise 3: Dipole field

Calculate the required flux density in the dipole of Exercise 2 for the carbon ion beam at $400\,\mathrm{MeV/u}$. The bending radius r_m of the dipole shall be $4.231\,\mathrm{m}$, and the bending angle shall be $22.5°$.

Exercise 4: Quadrupole field gradient

For a transfer line, which transports protons and fully stripped carbon ions C^{6+} with an energy of $7\,\mathrm{MeV/u}$ from a LINAC to a synchrotron, 6 quadrupole magnets are needed. Each quadrupole shall provide a quadrupole strength of $k = 2.8\,\mathrm{m}^{-2}$. Calculate the maximum required magnetic field gradient G.

Exercise 5: Iron saturation

The C-type dipole magnet in Fig. II.3.36 has an aperture height of $h = 100\,\mathrm{mm}$ and a pole width of $w = 250\,\mathrm{mm}$. The flux density plot shows a flux density in the aperture of $1.0\,\mathrm{T}$, but the back legs of the iron yoke are highly saturated and reach a flux density of almost $2\,\mathrm{T}$.

Why should saturation in the magnetic circuit (iron yoke) be avoided as much as possible? Give at least three arguments.

Calculate the necessary width of the back legs w_{leg} to ensure that the flux density in the iron remains below the saturation level of $1.5\,\mathrm{T}$.

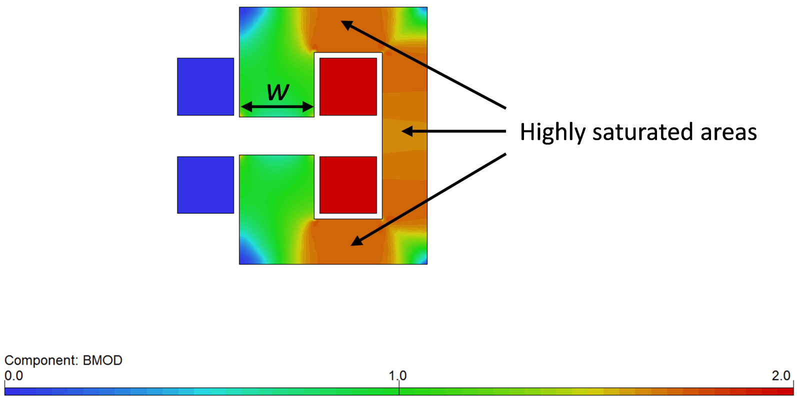

Fig. II.3.36: Exercise 5 - Iron saturation in the magnetic circuit. The magnetic flux density B_{mod} is indicated in units of tesla.

Exercise 6: Coil layout

A dipole magnet requires a total excitation current of 85 960 A (ampere-turns). The power converter can deliver a maximum current of $I_{\mathrm{max}} = 3000\,\mathrm{A}$. Calculate the number of turns per coil, assuming that the magnet has two coils connected electrically in series. Propose a coil layout defining the number of layers and the number of turns per layer.

Exercise 7: Pole design in a dipole

A straight R-bend dipole magnet with an aperture height of $h = 56\,\mathrm{mm}$ and a flux density in the aperture of $B = 1.43\,\mathrm{T}$ shall provide a field homogeneity of $\Delta B/B_0 = 5 \times 10^{-4}$ inside a good-field region with a horizontal width of $w_{\mathrm{GFR}} = \pm 20\,\mathrm{mm}$. The bending radius of the magnet is $r_b = 13.0\,\mathrm{m}$, and the bending angle is $\theta = 5°$.

Calculate the total pole width w_p for an optimised pole profile.

Exercise 8: Sextupole excitation

Derive the formula to calculate the excitation current NI (= ampere-turns per pole) for a sextupole, provided that the aperture radius r and the second derivative of the flux density B'' are known. Indicate in Fig. II.3.37 which integration path you have chosen.

A hint: In a sextupole, the field component B_y on the x-axis is parabolic, and $B'' = \frac{\mathrm{d}^2 B}{\mathrm{d}r^2}$ is constant.

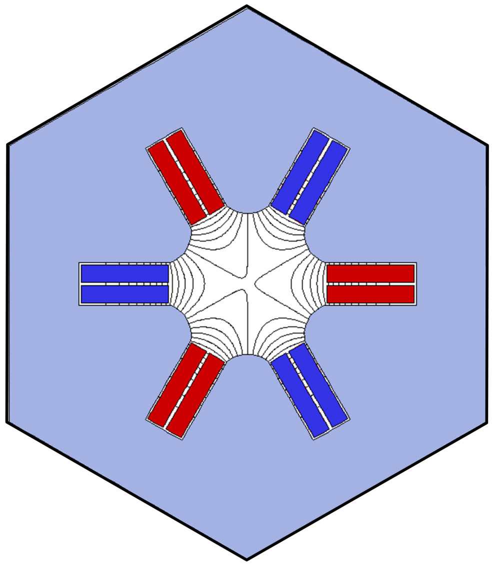

Fig. II.3.37: Exercise 8 - Cross section of a sextupole magnet with flux lines in the aperture.

Exercise 9: Power dissipated in a dipole coil

A dipole magnet is powered by a current of $I = 1720\,\mathrm{A}$. The magnet has two water-cooled coils connected electrically in series but hydraulically in parallel. Each coil has $N_T = 20$ turns, and the average conductor length per turn is $l_{\mathrm{avg}} = 3370\,\mathrm{mm}$. The two coils have an electrical resistance of $R = 4\,\mathrm{m}\Omega$ at room temperature $T_0 = 20\,°\mathrm{C}$. The temperature of the cooling water provided by the cooling plant is $T_{\mathrm{in}} = 25\,°\mathrm{C}$.

Calculate the dissipated power P_Ω at operating temperature, taking into account a maximum allowed temperature of $T_{\mathrm{max}} = 40\,°\mathrm{C}$ in the coils.

Exercise 10: Water cooling I

For the dipole in Exercise 9, compute the flow rate Q of the cooling water per coil (in litres per minute) required to remove the dissipated power. Also, calculate the cooling duct diameter provided that the cooling water station can handle a pressure drop of $\Delta P = 8\,\mathrm{bar}$.

Exercise 11: Water cooling II

Verify if the design from Exercise 10 respects the limits for the maximum allowed water velocity $v_{\mathrm{avg}} < 3\,\mathrm{m\,s^{-1}}$, and whether the flow is turbulent ($Re > 4000$).

Solutions

Solution 1

The positively charged proton is deflected in the positive x-direction.

Solution 2

The minimum beam energy is with protons at injection ($7\,\mathrm{M}e\mathrm{V}$). The corresponding beam rigidity can be calculated with the following formula

$$
\begin{aligned}
B_\rho(p) &= \frac{1}{Z\,e\,c}\sqrt{E_k^2 + 2\,E_k\,E_0} \\
&= \frac{1}{e\,c}\sqrt{(7\times10^6\,e\mathrm{V})^2 + 2(7\times10^6\,e\mathrm{V})(938\times10^6\,e\mathrm{V})} \\
&= 0.383\,\mathrm{T\,m}\,,
\end{aligned}
$$

using $c = 299.792\times10^6\,\mathrm{m\,s^{-1}}$ and $E_0 = 938\times10^6\,e\mathrm{V}$ for the proton rest mass energy.

For the maximum beam energy, we can rule out the $60\,\mathrm{M}e\mathrm{V}$ proton beam and the $120\,\mathrm{M}e\mathrm{V/u}$ carbon ion beam. For the two remaining options, we will need to compute the beam rigidity to find out which beam is more rigid. The beam rigidity for protons at 220 $\mathrm{M}e\mathrm{V}$ is

$$
\begin{aligned}
B_\rho(p) &= \frac{1}{e\,c}\sqrt{(220\times10^6\,e\mathrm{V})^2 + 2(220\times10^6\,e\mathrm{V})(938\times10^6\,e\mathrm{V})} \\
&= 2.265\,\mathrm{T\,m}\,,
\end{aligned}
$$

and for carbon ions at $400\,\mathrm{M}e\mathrm{V/u}$ it is

$$
\begin{aligned}
B_\rho(C^{6+}) &= \frac{1}{6\,e\,c}\sqrt{(12\times400\times10^6\,e\mathrm{V})^2 + 2(12\times400\times10^6\,e\mathrm{V})(12\times938\times10^6\,e\mathrm{V})} \\
&= 6.366\,\mathrm{T\,m}\,.
\end{aligned}
$$

As we can see, the most rigid beam is a carbon ion beam at $400\,\mathrm{M}e\mathrm{V/u}$. However, the magnet has to cover the full operation range from $7\,\mathrm{M}e\mathrm{V}$ protons to $400\,\mathrm{M}e\mathrm{V/u}$ carbon ions. This corresponds to a beam rigidity between $0.383\,\mathrm{T\,m}$ and $6.366\,\mathrm{T\,m}$ or a dynamic range of $1:16$.

Solution 3

To calculate the required flux density, we need the beam rigidity B_ρ of the carbon ion beam at $400\,\mathrm{M}e\mathrm{V/u}$ and the bending radius r_m of the dipole magnet:

$$
B = \frac{B_\rho}{r_m} = \frac{6.366\,\mathrm{T\,m}}{4.231\,\mathrm{m}} = 1.5\,\mathrm{T}\,.
$$

Solution 4

The maximum field gradient is needed for the carbon ion beam. The corresponding beam rigidity can be calculated with the help of

$$\begin{aligned} B_\rho(C^{6+}) &= \frac{1}{Z\,e\,c}\sqrt{E_k^2 + 2\,E_k\,E_0} \\ &= \frac{1}{6\,e\,c}\sqrt{(12\times 7\times 10^6\,e\mathrm{V})^2 + 2(12\times 7\times 10^6\,e\mathrm{V})(12\times 938\times 10^6\,e\mathrm{V})} \\ &= 0.766\,\mathrm{T\,m}\,, \end{aligned}$$

resulting in a maximum field gradient of

$$G = B' = B_\rho\,k = 0.766\,\mathrm{T\,m}\times 2.8\,\mathrm{m}^{-2} = 2.14\,\mathrm{T\,m}^{-1}\,.$$

Solution 5

Assuming that there is no significant stray flux outside the iron and the flux remains constant, the total flux Φ_f in the return yoke must be equal to the flux Φ_F in the air gap:

$$\Phi = B\,(w+2h) = B_{\mathrm{yoke}}\,w_{\mathrm{leg}}\,.$$

Therefore

$$w_{\mathrm{leg}} = \frac{B}{B_{\mathrm{yoke}}}\,(w+2h) = \frac{1.0\,\mathrm{T}}{1.5\,\mathrm{T}}\,(250\,\mathrm{mm} + 2\times 100\,\mathrm{mm}) = 300\,\mathrm{mm}\,.$$

Solution 6

With a 10% margin on the maximum current of the power converter, we get the nominal current for the magnet:

$$I_{\mathrm{nom}} = 0.9\times I_{\mathrm{max}} = 0.9\times 3000\,\mathrm{A} = 2700\,\mathrm{A}\,.$$

One coil has $85\,960/2 = 42\,980$ ampere-turns. The number of turns per coil is

$$N_T = \frac{42\,980\,\mathrm{A}}{2700\,\mathrm{A}} = 15.92\,\mathrm{turns}\,.$$

The next largest integer is 16 turns, which can be divided into 2 layers of 8 turns each. The nominal current has to be recalculated for 16 turns:

$$I_{\mathrm{nom}} = \frac{42\,980\,\mathrm{A}}{16} = 2686\,\mathrm{A}\,.$$

This leaves a margin of 315 A ($> 10\%$) with respect to the maximum current of the power converter.

Solution 7

The total pole width w_p can be calculated using

$$w_p = 2\left(w_{\mathrm{GFR}} + x_p\right) + s = 2\left(w_{\mathrm{GFR}} + \frac{h}{2} f\left(\frac{\Delta B}{B_0}\right)\right) + s\,,$$

with

$$f\left(\frac{\Delta B}{B_0}\right)_{\mathrm{opt.}} = -0.14\ln\left(5\times10^{-4}\right) - 0.25 = 0.814\,,$$

and

$$s = r_b\left(1-\cos\left(\frac{\theta}{2}\right)\right) = 13\,\mathrm{m}\left(1-\cos\left(\frac{5^\circ}{2}\right)\right) = 12.4\times10^{-3}\,\mathrm{m} = 12.4\,\mathrm{mm}\,.$$

The final width of the optimised pole yields

$$w_p = 2\left(20\,\mathrm{mm} + \frac{56\,\mathrm{mm}}{2}0.814\right) + 12.4\,\mathrm{mm} = 98\,\mathrm{mm}\,.$$

Solution 8

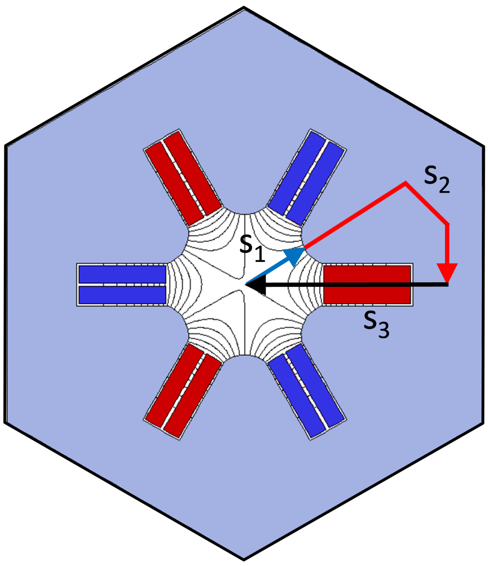

Fig. II.3.38: Solution 8 - Cross section of a sextupole magnet with integration path $\oint H\,\mathrm{d}s$ to calculate the ampere-turns NI.

To identify the required number of ampere-turns for a sextupole, we use the same approach as for quadrupoles. In a sextupole, the field component B_y on the x-axis is parabolic, and $B'' = \frac{\mathrm{d}^2B}{\mathrm{d}r^2}$ is constant so that

$$H(r) = \frac{B''}{2\mu_0}r^2$$

leads to

$$NI = \oint H\,\mathrm{d}s \approx \int_0^R H(r)\,\mathrm{d}r = \frac{B''}{2\mu_0}\int_0^R r^2\,\mathrm{d}r$$

and to

$$NI_{(\text{per pole})} = \frac{B'' r^3}{6\mu_0}\,.$$

Solution 9

The maximum allowed temperature increase in the water-cooled coil is $\Delta T = T_{\mathrm{max}} - T_{\mathrm{in}} = 15\,^\circ\mathrm{C}$, and therefore the average temperature increase is $7.5\,^\circ\mathrm{C}$. So, we can calculate the resistance at operating temperature using

$$R = R(T_0)\,(1+\alpha\,(T_{\mathrm{avg}} - T_0)) = 2.0\,\mathrm{m}\Omega\left(1 + 0.004\,\mathrm{K}^{-1}\,(32.5\,^\circ\mathrm{C} - 20\,^\circ\mathrm{C})\right) = 2.1\,\mathrm{m}\Omega\,.$$

The dissipated power in one coil is

$$P_\Omega = RI^2 = 2.1\times10^{-3}\Omega \times (1720\,\mathrm{A})^2 = 6213\,\mathrm{W} = 6.21\,\mathrm{kW}\,.$$

Solution 10

For this exercise, we use non-Si units for the flow rate $[Q] = 1\,\mathrm{L\,min}^{-1}$, pressure drop $[\Delta P] = 1\,\mathrm{bar}$, and cooling hole diameter $[d_h] = 1\,\mathrm{mm}$. The required cooling flow rate per coil is

$$Q = 14.5\frac{P_\Omega}{\Delta T} = 14.5\frac{6.21\,\mathrm{kW}}{15\,^\circ\mathrm{C}} = 6.01\,\mathrm{L\,min}^{-1}\,.$$

The necessary cooling hole diameter is

$$d_h = 2.31\,Q^{0.368}\left(\frac{l_h}{\Delta P}\right)^{0.21} = 2.31\left(6.01\,\mathrm{L\,min}^{-1}\right)^{0.368}\left(\frac{20\times 3.37\,\mathrm{m}}{8\,\mathrm{bar}}\right)^{0.21} = 7.0\,\mathrm{mm}\,.$$

Solution 11

The average water velocity can be computed directly from the required cooling flow rate using

$$v_{\mathrm{avg}} = 16.67\frac{Q}{a_h} = 66.67\frac{Q}{d_h^2\pi} = 66.67\frac{6.01\,\mathrm{L\,min}^{-1}}{(7\,\mathrm{mm})^2\,\pi} = 2.61\mathrm{m\,s}^{-1}\,,$$

and is hence clearly below the limit of $v_{\mathrm{avg}} < 3\,\mathrm{m\,s}^{-1}$. The Reynolds number of

$$Re = d_h\frac{v_{\mathrm{avg}}}{\nu}10^{-3} = 7\,\mathrm{mm}\frac{2.61\,\mathrm{m\,s}^{-1}}{6.982\times10^{-7}\,\mathrm{m}^2\,\mathrm{s}^{-1}}10^{-3} = 27\,711$$

indicates that the flow is in the turbulent range.

Case study

This case study aims to apply the subjects discussed in the theoretical part, particularly the sections about analytical design. To make this study as realistic as possible, we will take a magnet designed and built for MedAustron—a medical accelerator and ion therapy centre for cancer treatment and clinical research in Austria [8]. Such a case study is usually given to the students during the JUAS lectures; they are asked to work out possible solutions in small groups and present their findings at the end of the lecture series.

Like in real life, not all parameters will be given explicitly, so we must make reasonable assumptions to progress in the design process. Of course, these assumptions always have to be cross-checked and scrutinised at the end to ensure they do not contradict the initial requirements and constraints.

II.3.6.4 Introduction

MedAustron is located in Wiener Neustadt, 50 km south of Vienna. The main activities are related to tumour treatment and clinical research, but also nonclinical research, like radiation physics and radiation biology, is supported to a certain extent.

The accelerator is synchrotron-based and has a circumference of 76 m. For medical applications, the facility can produce proton beams with energies between 60 and 250 $\mathrm{M}e\mathrm{V}$ and carbon ion beams with energies from 120 to 400 $\mathrm{M}e\mathrm{V/u}$. Proton beams with higher energies of up to 800 $\mathrm{M}e\mathrm{V}$ can be provided for experimental physics. Optionally and at a later stage, the use of other ions with a charge-to-mass ratio of $q/m > 1/3$ will be possible. Figure II.3.39 shows a footprint of the beamlines and treatment rooms at the MedAustron facility.

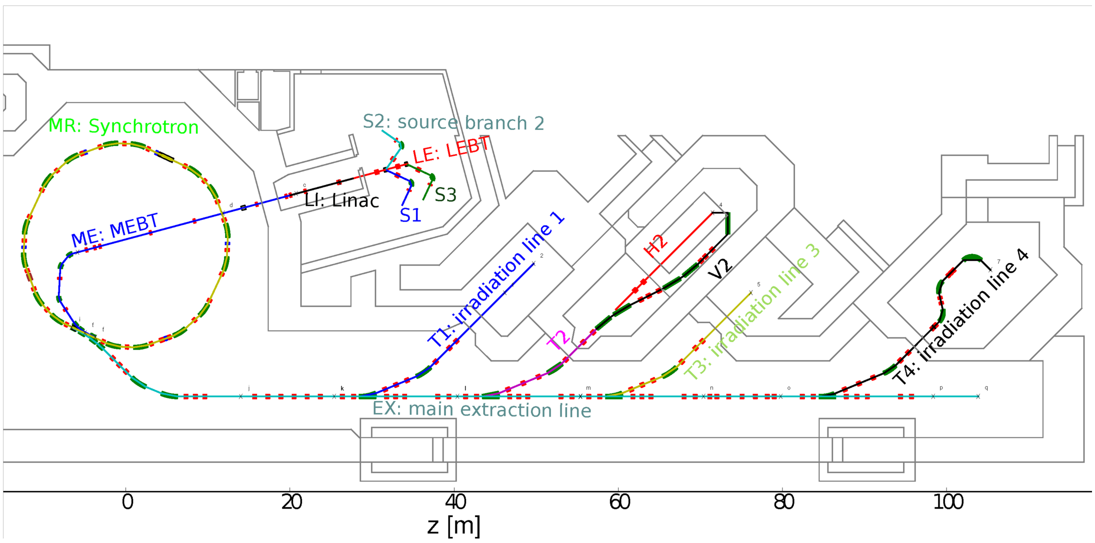

Fig. II.3.39: Footprint of the MedAustron facility showing the three ion sources, the LINAC part, the synchrotron, the extraction beamlines, and the four treatment rooms.

Almost 300 magnets of more than 20 different types were built for MedAustron's entire magnet system. This includes solenoids, spectrometer magnets, bending dipoles, vertical and horizontal steering magnets, quadrupoles, sextupoles, scanning magnets, a betatron core, and a large gantry magnet. The magnet type selected for this case study is a bending magnet for the medium-energy beam transfer

(MEBT) line.

II.3.6.5 Requirements and constraints

The functional specification requires three bending dipoles for the MEBT line between the LINAC and the synchrotron. These magnets direct the protons and C^{6+} ions towards the injection region of the synchrotron (see Fig. II.3.40). A summary of the beam parameters can be found in Table II.3.5.

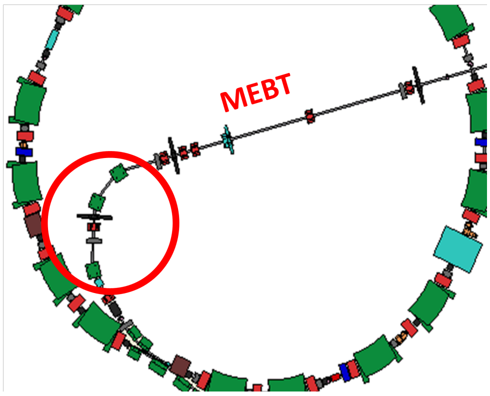

Fig. II.3.40: Footprint of the MedAustron medium-energy beam transfer (MEBT) line with the three bending magnets.

Table II.3.5: Beam parameters of the MedAustron MEBT line

Parameter	Value
Particle type	Protons, C^{6+}
Beam energy	7 MeV/u
Length of beamline	40.9 m
Beta function β_x, β_y	$\approx$ 10 m
Beam size σ_x, σ_y	$\pm$10 mm

The three dipoles together shall provide a total bending angle of $\theta_t = 108°$ for both ion species. The beam entry and the beam exit angles with respect to the pole end faces shall be $\Psi = \pm 72°$, which means that the magnet shall have parallel end faces. The overall mechanical length, including yoke, coil heads, and connections, is restricted to $l_{\text{mech}} = 0.9$ m per magnet.

The required field homogeneity $\Delta B/B_0$ within the good-field region shall be better than $\pm 1 \times 10^{-3}$. The good-field region shall be $GFR_h = \pm 30$ mm in horizontal direction and $GFR_v = \pm 23$ mm in vertical direction.

The magnets are operated in quasi-static mode with a field ramp rate of less than $0.3\,\text{T}\,\text{s}^{-1}$, and the three dipoles are electrically connected in series. The power converter can deliver a maximum current of $I_{\text{max}} = 600$ A and a voltage of $U_{\text{max}} = 100$ V. A water cooling station is available, which can provide demineralized water to the magnets with a temperature of $T_{\text{in}} = 25°$C and a pressure of $P_{\text{in}} = 10$ bar but requires a minimum return pressure at the magnet outlet of $P_{\text{out}} = 2$ bar. For advanced operation stability, the temperature increase in the magnet coils ΔT shall be kept below 15°C. The constraints and requirements are summarised in Table II.3.6.

Table II.3.6: Magnet parameters of the MedAustron MEBT dipoles.

Parameter	Value
Number of magnets in series	3
Bending angle Θ per magnet	36°
Max. mechanical length l_{mech} per magnet	0.9 m
Operation mode	quasi-static
Field ramp rate $\mathrm{d}B\,/\,\mathrm{d}t$	$0.3\,\mathrm{T\,s^{-1}}$
Horizontal good-field region GFR_h	±30 mm
Vertical good-field region GFR_v	±23 mm
Field quality $\Delta B/B_0$ inside GFR	$\pm 1 \times 10^{-3}$
Max. power converter current I_{max}	600 A
Max. power converter voltage U_{max}	100 V
Available cooling water pressure P_{in}	10 bar
Required return pressure P_{out}	2 bar
Cooling water temperature T_{in}	25°C
Max. temperature increase ΔT	15°C

II.3.6.6 Additional information

The total quantity of steel required for the entire project was supplied by one steel manufacturer. MedAustron decided to use steel strips of grade M1200-100A with insulating epoxy coating for all magnets. The MEBT magnet yokes shall be built from laminated steel of this type.

A stock of different copper conductor types was left over from the production of other MedAustron magnets. All types have a square cross section and circular cooling duct in the centre. If possible, the MEBT magnet coils shall be made from one of the conductors listed in Table II.3.7.

Table II.3.7: Dimensions of available copper conductor types.

Type	Copper grade	Outer dimensions	Cooling duct diameter	Edge radius	Available length
Type 1	OF-Cu	25 mm × 25 mm	12.0 mm	1.5 mm	≈ 300 m
Type 2	OF-Cu	11 mm × 11 mm	5.5 mm	1.0 mm	≈ 600 m
Type 3	OF-Cu	11 mm × 11 mm	5.0 mm	1.0 mm	≈ 800 m
Type 4	OF-Cu	8 mm × 8 mm	5.0 mm	1.0 mm	≈ 500 m

In addition to the three magnets to be installed in the transfer line, one complete spare unit is required. The basic analytical and conceptual design is necessary to derive the most important parameters of the magnet and should include at least the following:

– Yoke shape: straight or curved
– Yoke type: C-shape or H-shape
– Flux density B in the aperture

– Aperture height h
– Yoke length l_{yoke} and magnetic length l_{eff}
– Pole width w and return yoke thickness
– Excitation current or ampere-turns NI
– Coil cooling: water cooling or air cooling
– Nominal current I and number of turns N_T
– Conductor dimensions and current density J
– Coil size: coil width, coil height, insulation thickness, conductor length
– Coil resistance R and dissipated power P_Ω
– Coolant flow rate Q and required pressure drop ΔP for cooling water
– Average coolant velocity v_{avg} and Reynolds number Re

Apart from the parameters mentioned above, the analytical design should first provide an idea of the yoke and coil geometry for the numerical design phase. To facilitate the preparation of the numerical model, it is a good practice to produce a sketch or a list identifying the x and y-coordinates of the key points as shown in Fig. II.3.41 (red dots). These coordinates should be provided with respect to the beam axis, which is typically identical to the centre of the magnet aperture.

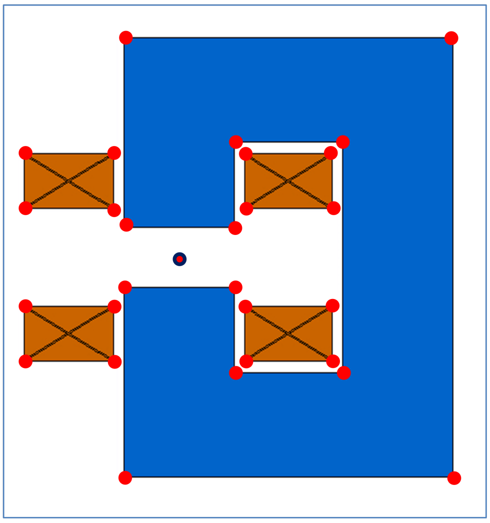

Fig. II.3.41: Possible cross section of the MedAustron MEBT dipole indicating the most important key points to be calculated.

All this information, together with the results from the numerical simulations, shall be eventually summarised in a detailed magnet design report. This document shall describe the entire design process, explain the reasoning for each design choice, and provide evidence that all input requirements and constraints have been respected in the final magnet layout.

Bibliography

The following bibliography lists recommended scientific literature for further exploration.

J.T. Tanabe, *Iron dominated electromagnets* (World Scientific, Singapore, 2005), doi:10.1142/5823.

G. Parzen, *Magnetic field for transporting charged beams*, BNL-50536 (Brookhaven National Lab., Upton, NY, 1976), doi:10.2172/7254841.

S. Russenschuck, *Field computation for accelerator magnets: Analytical and numerical methods for electromagnetic design and optimization* (Wiley, Weinheim, 2010), doi:10.1002/9783527635467.

K. Wille, *The physics of particle accelerators: An introduction* (Oxford University Press, Oxford, 2000).

H.E. Knoepfel, *Magnetic fields: A comprehensive theoretical treatise for practical use* (Wiley, New York, 2000), doi:10.1002/9783527617418.

D. Brandt (ed.), *CAS - CERN Accelerator School: Specialised course on magnets, Bruges, Belgium 16–25 Jun. 2009*, CERN-2010-004 (CERN, Geneva, 2010), doi:10.5170/CERN-2010-004.

S. Turner (ed.), *CAS - CERN Accelerator School: Measurement and alignment of accelerator and detector magnets, Anacapri, Italy 11–17 Apr. 1997*, CERN-1998-005 (CERN, Geneva, 1998), doi:10.5170/CERN-1998-005.

S. Turner (ed.), *CAS - CERN Accelerator School: Magnetic measurement and alignment: Montreux, Switzerland 16–20 Mar. 1992*, doi:10.5170/CERN-1992-005.

References

[1] Britannica, The Editors of Encyclopaedia, "magnetic field strength", Encyclopedia Britannica, 12 Aug. 2024, https://www.britannica.com/science/magnetic-field-strength, Accessed: April 2024.

[2] S. Zurek, "Magnetisation", Encyclopedia Magnetica, https://www.e-magnetica.pl/doku.php/magnetisation, Accessed: April 2024.

[3] DIN EN 10106:2016-03, Cold rolled non-oriented electrical steel strip and sheet delivered in the fully processed state; German version EN 10106:2015.

[4] D. Tommasini, *Practical definitions & formulae for normal conducting magnets*, Internal note 2011-18 (CERN, Geneva, 2011), EDMS 1162401.

[5] J.T. Tanabe, *Iron dominated electromagnets* (World Scientific, Singapore, 2005), doi:10.1142/5823.

[6] J.H. Lienhard IV and J.H. Lienhard V, *A heat transfer textbook, third edition*, Phlogiston Press (2003).

[7] L.F. Moody, *Friction factors for pipe flow*, Transactions of the ASME, 66 (8): 671–684 (1944).

[8] MedAustron - Ion Therapy Center, https://www.medaustron.at, Accessed: April 2024.